Calculation and comparison of linear energy transfer and relative biological effectiveness in proton therapy using FLUKA Monte Carlo simulations and the ECLIPSE treatment planning system

Khaled Mohamad Katmeh

Supervisors:

Kristian Smeland Ytre-Hauge

Tordis Johnsen Dahle

Master thesis in medical physics and technology

Department of Physics and Technology

University of Bergen

December 2020

Acknowledgements

I would start by thanking my supervisors, Ph.D. Kristian Smeland Ytre-Hauge and Ph.D. Tordis Dahle.

Thank you, Ph.D. Kristian Smeland Ytre-Hauge, for submitting me with this interesting project and giving me all the needful tools and revelation for writing this master thesis.

Thank you, Ph.D. Tordis Dahle for dialogues that helped me to complete this project and verify the extent of the results.

I would also like to thank Professor Dieter Röhrich for your interesting lectures about particle therapy within the stage of master's study.

Certainly, I will not forget Ph.D. Mamdouh Chaar for all the assistance he provided to me, the meetings that took place in his office, and the discussions that helped overcome some of the obstacles in the study period.

I thank all staff in the Department of Physics and Technology especially the section of Medical Physics to provide the facilities and tools required for research.

And lastly, with decisive, a special thanks to my darling parents Hind Kalaleeb and Mohamad Katmeh, dear brothers Ameer and Hamza, wonderful wife Marah Albared, and to my little angel Mohamad to support and stand by me, I will always appreciate it.

Abstract

Currently, the world turns toward using charged particle radiotherapy, as protons and heavy ions share an advantage to achieve a more conformal physical dose distribution to the tumour than the conventional methods by photons. There is increased demand in a scientific community of moving from a relative biological effectiveness, RBE, of 1.1 for protons and to step aside from this generic-value through consistency by a linear energy transfer, LET, and make validation of one of RBE models to investigate how LET calculation can be used in the treatment planning process. The LET and RBE will investigated for a water-phantom and brain tumor patient case in this project.

The scientific community notably distinguished of Bragg-peak phenomenon which have higher LET value and simultaneously helping to avoid the co-irradiation of normal tissue compared to conventual radiotherapy features of low-LET value. The charged particles therapy of higher of LET value concentrates to the tumour that resistant of conventual radiotherapy and to tumour nearby location to critical organs, it used this type of treatment clinically limited of certain tumour kinds, for instance, skull base tumours, pediatric tumours, due to there is difficulty predict precisely of side effects on long-term like second malignant or hazard of late normal tissue harm. Protons have higher biological effect compared to photons, which is clinically representatives by a generic relative biological effectiveness (RBE), equal 1.1.

The biological effect or namely, RBE, mainly relies on the manner of the density of ionization actions along the track of radiation namely the absorbed dose distribution and LET, where studies showed at the distal end of the proton beam the RBE value is rising with the rise in value of LET. In proton therapy, two methods utilized for delivering the treatment through passive scattering or pencil beam scanning, the latter is the most current state and widely used which can lead to higher average LET, with

perhaps additional biological effects due to variations in how the protons are modulated compared with passive scattering. In the original treatment plan when computing the relative biological effectiveness (RBE) does not bear in mind the LET. The accuracy of delivery prescription dose in trade treatment planning systems (TPS) renounce in order to capitalize on the TPS calculation in a reasonable time-scale. At present, Monte Carlo (MC) code simulations are the gold standard in dose calculation, but its use in clinical work is still limited due to the long computational time needed. The FLUKA MC tool has been used for recalculation of dose, LET and RBE distributions in this work. A prototype LET estimator integrated into FLUKA was also used.

The aim of this work is to recalculate the biological dose of TPS by FLUKA MC and calculate the corresponding LET using FLUKA and Eclipse utilizing a script called Micro-Calculation especially for Eclipse in order to LET calculation as well as inspect the RBE-McNamara model values at LET for both techniques, and verify this.

The results showed relatively good agreement for the comparison of biological dose between FLUKA MC and Eclipse (TPS), through utilized the Micro-Calculation script in Eclipse software to calculate the LETd value gave higher outcomes than FLUKA MC calculated in some of the studied organs. The RBE-MCN values was for the good of calculated of FLUKA MC than the Eclipse Micro-Calculation for all studied cases generally, where RBE value was not constant at 1.1 generic value.

Contents

1. Introduction

Cancer is a group of diseases characterized by cells beginning to divide without stopping and spread of abnormal cells into surrounding tissues. There are over 100 types of cancer (National Cancer Institute, 2015). Many people around the world are infected with cancer, often leading to premature death when diagnosis and treatment are not done right. Cancer is the second leading cause of death globally and is responsible for an estimated 9.6 million deaths in 2018. Globally, about 1 in 6 deaths is due to cancer (World Health Organization, 2018,September).

There are many ways to treat cancer. Treatment can include chemotherapy, hormone therapy, surgery, immunotherapy and radiotherapy. These treatments can be used separately or in combination. The type of treatment will depend on the type of cancer (Institute, 2019,July). Radiotherapy plays a major role in cancer care, a correct and early diagnosis gives a better chance of survival as this can determine the extent and location of cancer, which helps specialists determine cancer type and appropriate treatment method (Institute, 2019,July).

There are several methods to help disclose cancer that can assist doctors in diagnosis, for instance, laboratory tests made by blood or urine tests, biopsy as the doctor gathers samples of cells for testing or by imaging tests, allow to generate pictures of regions inside the patient bode, the pictures can be made in a few different ways like magnetic resonance imaging (MRI), computed tomography (CT) scan, positron emission tomography (Yamoah & Johnstone) scan, X-ray and ultrasound. Under of the computerized development that has taken place in recent years, revolutionary progress has been made in the treatment of radiation oncology, these developments have helped to make radiography more accurate in the three spatial and fourth (temporal) dimensions, computerized planning systems have also helped to makes 3D measurements more ease and accuracy.

One of the methods in radiotherapy is external radiation therapy, the patient irradiated from the outside by photon or heavy particles. The aim of radiotherapy is to eliminate cancer cells by delivery of enough doses to the target and avoid the surrounding healthy tissue at the same time. The heavy particles usually utilize to irradiate due to their characteristic as know Bragg peak has virtually no exit dose. The successful treatment depends on many factors, one of the factors determining the success of radiation therapy is determining the appropriate and sufficient dose for the target, diagnostic medical imaging is carried out through one of the methods mentioned above previously and consequently determines the volume of the target whereupon the dose calculation is based (Khan & Gibbons, 2014).

1.1 Radiotherapy

Radiotherapy is a treatment utilized ionizing radiation aiming to deliver an adequate and uniform dose to kill cancer or malignant cells and to achieve tumor control, while meanwhile, as far as possible, avoid normal organs and healthy tissue.

Radiotherapy can be delivered both internally or as external radiotherapy: In internal radiotherapy, also called brachytherapy, radioactive sources are implanted inside the patient. In external radiotherapy radiation from a source outside the patient is used. This can be from a radioactive source or from equipment such as a linear accelerator (LINAC). The radiation can be photons (x-rays), electrons, and heavy charged particles such as protons or carbon ions (Use, 2008).

There are various types of external radiotherapy, all share the aim of delivery of the required rays to the tumor while avoiding the normal tissues around it. Each type depends on a

method for calculating and analyze images of the tumor to account the dose and the accurate way of treatment, examples of these types:

I. 3D Conformal Radiotherapy (CRT), this implies that beams are uniquely shaped to fit the infected region. In 3D CRT the radiation beams used in treatments are of uniform intensity across the field (Webb, 1997).

II. Intensity-Modulated Radiotherapy (IMRT) allows for better tumor inclusion and sparing normal tissue than 3D CRT, as in IMRT the intensity beam profile is modified and delivered with nonuniform fluence using dynamic multileaf collimators (MLC), which can shape the treatment area with high precision and avoid the vital organ of the radiation dose (Khan & Gibbons, 2014).

III. Volumetric-Modulated Arc Radiotherapy, VMAT, is a more modern form of IMRT, in this radiation therapy technique the LINAC machine rotates continuously during delivery of the radiation dose and changes the intensity of the radiation beam according the treatment area. This makes VMAT progressively precise and abbreviate the treatment time (Teoh, Clark, Wood, Whitaker, & Nisbet, 2011).

IV. Image-Guide Radiotherapy, IGRT, is the use of imaging during radiation therapy to improve the precision and accuracy of treatment delivery. Radiation therapy machines, LINAC, merge with imaging technologies like CT to image the tumor before and during the treatment (Jaffray, 2012).

V. Four-Dimensional Radiotherapy, 4D Radiotherapy, previous methods of radiotherapy may not always be safe for normal tissues that are adjacent, especially tumor sites in the thorax and abdomen due to respiration process. This leads to difference between the planned and presented doses and the inaccuracy of the hit the target. By monitoring motion, time is added as a fourth dimension to track the motion of patient (Gui, Feng, Yi, Dhople, & Yu, 2010).

VI. Stereotactic Radiotherapy, SRT, is good choice for small tumor or cancer due to the method is of focused many beams towards a tumor at different angles. There are two types of stereotactic radiation:

1- stereotactic Radiosurgery, (SRS), for brain.

2- stereotactic Body Radiotherapy, (SBRT), for all body (Song, Park, Griffin, & Levitt, 2011).

1.2 Proton Therapy

Robert R. Wilson is the physicist that in 1946 suggested using protons in radiotherapy. Wilson showed the advantages of protons compared with conventional photon therapy. He outlined the idea for treating tumors utilizing the finite range and the Bragg peak of proton beams (Bragg & Kleeman, 1905; Wilson, 1946).

The concept of proton therapy was not immediately implemented at Wilson's home institution at Harvard University, however, after a couple of years, Lawrence Berkeley Laboratory (LBL) in California applied the concept and treated the first patient in 1954 (Lawrence, 1957). Other ions such as helium and carbon ions were also applied in therapy, and the term particle therapy is used to describe radiotherapy with accelerated ions.

After the first patient treated by proton therapy at LBL, in 1955 Gustav Werner Institute in Sweden started medical use of protons and arrangement of animal's tests were performed to study the biological effect of proton radiation and in 1957 the first patient was treated using a 185-MeV cyclotron (Chaturvedi et al., 2007; Hawkins, Draper, & Kingston, 1987; Rydberg, 1996). The merit of proton radiation therapy compared with conventional photon radiation therapy made the world more interested in using proton therapy in cancer treatment.

Today, 103 proton therapy centers are clinically active worldwide, and many more are under planning, including two centers in Norway. Over 180 000 patients worldwide has been

treated with particle therapy, as reported by the Particle Therapy Co-Operative Group (Group).

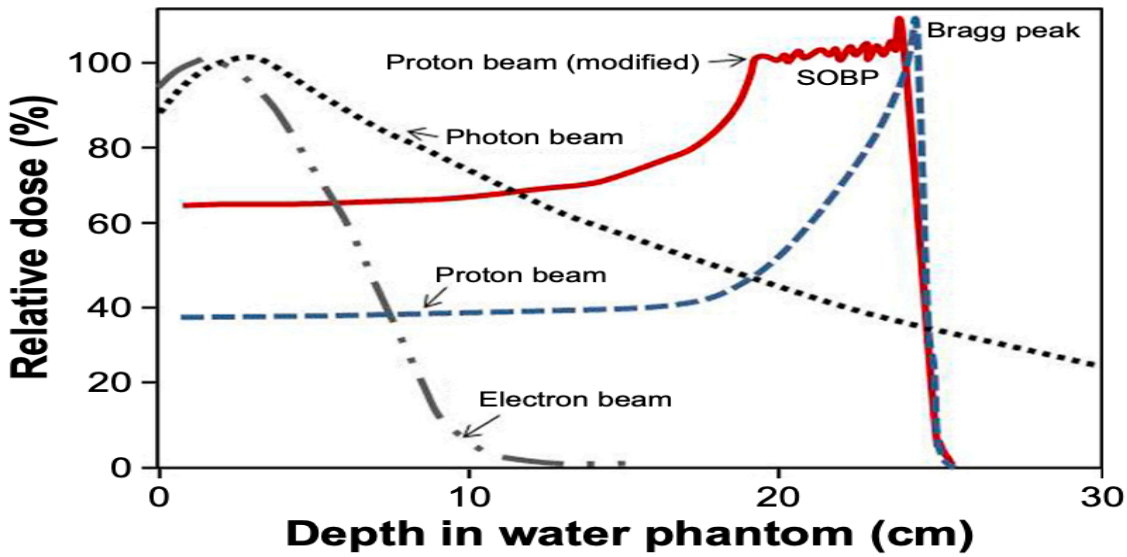

Figure 1. Comparison of relative depth dose distribution of protons in a water phantom versus photons and electrons, the blue dashed line representing the energy distribution of the proton beam as a function of depth in a target. the Black dotted indicate for photon distribution as a function of depth. Gray dotted/dashed line plots the electron distribution as a function of depth. Red-line outlines the combination of multiple proton beams, forming a spread-out Bragg peak (SOBP) for protons (Yamoah & Johnstone, 2016).

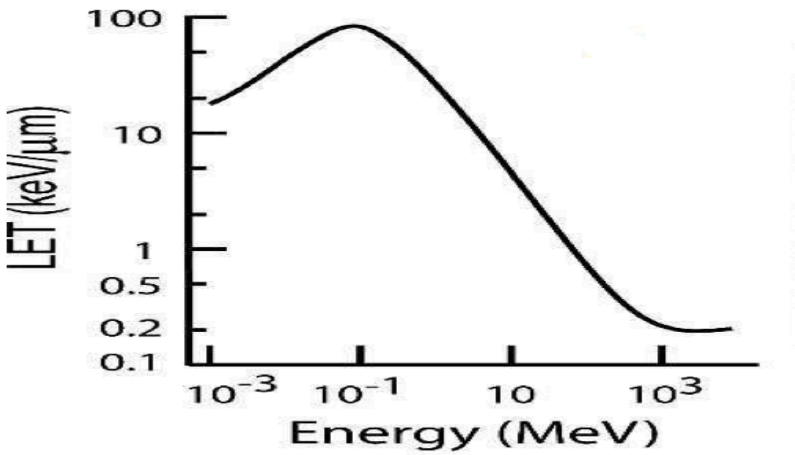

Figure 2. Linear energy transfer of the proton as a function of the kinetic energy(Girdhani, Sachs, & Hlatky, 2013).

The finite range of a proton beam is the most distinguished difference between photon and proton beams. In addition, as protons penetration through the matter, the velocity of the protons is reduced due to the interaction with the matter and this causes the dose deposition of protons to increase with depth until the energy of the protons is completely exhausted and they stop. This leads to a maximum dose deposition at a certain depth in matter with a peak and then a sharp drop off in dose distal to the peak. The peak is called the "Bragg peak" (Tayama et al., 2002). This is unlike photons and electrons where the build-up deposition dose region at the initial of their path and dose deposition decreasing after the build-up region as distance increases in the matter (Mohan, Mahajan, & Minsky, 2013; Yamoah & Johnstone, 2016).

Protons and photons have different biological effectiveness, concept of the relative biological effectiveness (RBE) was introduced to represent the different biological effects, defined as the ratio between the dose from 60Co γ-rays and dose from another radiation that produces the same biological end-point. In clinical proton therapy, a generic RBE of 1.1 is currently used. However, according to experimental data, the RBE of protons is not constant, and in vitro irradiation experiments has shown that the RBE depends on many factors like physical dose, linear energy transfer (LET), and (α/β)-ratio of the Linear Quadratic (LQ) model (Harald Paganetti et al., 2002). The LET describes the energy lost/deposition per unit path length along with the particle track and is handily expressed in units of keV/μm. The LET decrease as the proton energy increases as Figure 2 shows and therefore depends on the particle energy (Mori, Sakae, Takada, & Takei, 2020).

1.3 Project Objectives/Motivation

There is an increasing consensus in the scientific community that using an RBE of 1.1 is insufficient and that the variations in RBE with LET should be taken into account in proton

therapy. Until recently, LET has only been available through the use of general-purpose Monte Carlo codes. However, prototype LET estimators are now becoming available in commercial treatment planning systems (TPS).

The biological effects in radiotherapy need careful evaluation to achieve the treatment with fewer disadvantages, and regardless of the increasing use of proton therapy there stay two critical uncertainties related to proton therapy: The insufficient information of relative biological effectiveness, RBE, at various doses and in various tissues and accuracy of Bragg peak position (B. Jones, 2015). For proton therapy treatment, the RBE-weighted or so-called biological dose considered as the key for determining dose prescription in proton therapy (Beyzadeoglu, Ozyigit, & Selek, 2012). The relative biological effect computation is difficult since it depends on linear energy transfer and the type of tissue response must be known with high precision (Harald Paganetti, 2003).

Since of the significant importance of performing the linear energy transfer and related relative biological efficacy with dose in proton therapy treatment, this study aims to compare proton dose and LET calculations from the Eclipse treatment planning system (TPS) and FLUKA Monte Carlo (MC). These LET estimators has been used separately before but a comparison of the two has not been done. On one hand, the MC approach is considered the most reliable, but is difficult to apply in a clinical setting. It is therefore of high importance to investigate if there is agreement or differences between the two methods.

2. Physics of Particle Therapy

In medical physics, the charged particles (protons and light ions) in radiation therapy is one of the most successful cases for treating cancer without external surgical intervention. The biological properties of ionizing radiation in addition to the physical features in terms of accuracy make charged particles a favorable choice in clinical terms (G Battistoni, Mattei, & Muraro, 2016). The principle of particle therapy is based on the interaction of charged particles with matter and they deposit their energy to a specified target through ionizing the target atoms (Lomax, 2009). The basic interaction of protons with matter will be shown in this chapter.

2.1 Interactions

Materials consists of atoms and it constitutes a mixture of electrons and nuclei. Protons, and other charged particles interact with the electrons and nuclei and lose their energy during the interaction in different mechanisms: inelastic interaction with atomic electrons, elastic interactions with atomic nucleons, nuclear interaction with nucleus and Bremsstrahlung (Tsuboi, 2020), the latter case effect is negligible at therapy proton (Newhauser & Zhang, 2015). The interactions are illustrated in Figure (3).

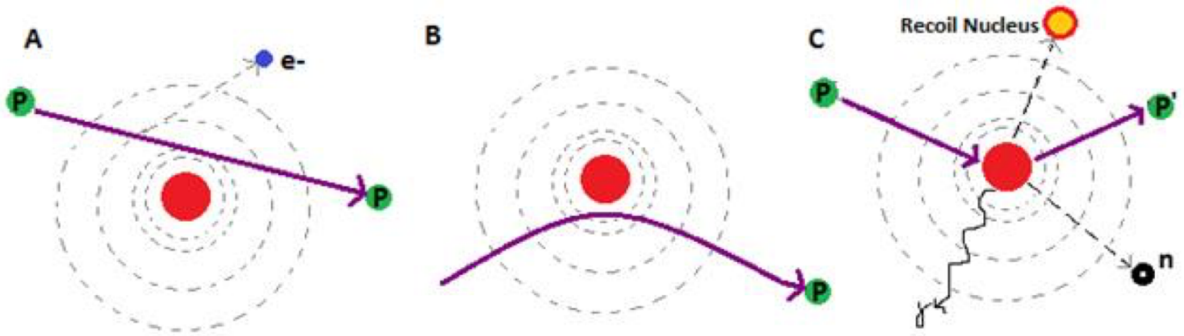

Figure 3. Illustration of three proton interaction processes. A) the proton energy loss based on inelastic Coulomb interaction. B) The proton deviation from trajectory due to repulsive Coulomb elastic scatter with the nucleus. C) The proton deviation from trajectory due to repulsive Coulomb elastic scatter with the nucleus, resulting in formation of secondary particles and removal of the primary proton by nuclear interaction (Newhauser & Zhang, 2015).

2.1.1 Inelastic interactions with atomic electrons

Interaction the protons and atomic electrons by Coulomb interaction represents the basic process, causing atomic exciting or ionizing with negligible deflection of the primary proton due to proton mass being 1843 times greater than the electron mass (Newhauser & Zhang, 2015; Park & Kang, 2011).

The energy transferred from proton to electron at each interaction is considered a tiny amount of energy to release the electron from an atom, i.e. ionization, the recoil electrons that have low kinetic energy precipitation their energy locally (Takei, 2020). There are a few electrons that get enough energy to ionize nearby atoms by a process called second ionization, these electrons are known as δ-rays (Takei, 2020).

The protons lose their kinetic energy as a result of interactions during the movement time in the medium. The medium has the capability to stop protons and this capability known as linear stopping power and denotes by S, and it described the energy loss of charged particle, dE ,per unit of track, dx, thus

$$S = -\frac{dE}{dx}.$$

The stopping power has unit $^{MeV}/_{m}$.

S consisting of three parts, S_{el} , S_{rad} and S_{nuc}:

$$S = -\left[\left(\frac{dE}{dx}\right)_{el} + \left(\frac{dE}{dx}\right)_{rad} + \left(\frac{dE}{dx}\right)_{nuc} \right]$$

S_{el} is the electronic stopping power in respect of inelastic interactions with atomic electrons, S_{rad} is the radiative stopping power due to Bremsstrahlung, S_{nuc} is the nuclear stopping power because of elastic Coulomb interaction with the target nuclei. For non-elastic nuclear interaction mechanisms are not usually described by a stopping power (Thomas, 2012). The electronic stopping power is the dominant process and for nuclear stopping power becomes important for heavier particles than the proton, the radiative stopping power contribution is lower than elastic Coulomb interaction with the target nuclei so can be neglected for therapeutic protons, we get $S = -\left(\frac{dE}{dx}\right)_{el}$ (Elia, 2019).

Bethe (Bethe, 1930) and Block (Bloch, 1933) developed the theory of the proton energy loss which considers the electronic stopping power is the dominated process (Elia, 2019), the equation expressed as Bethe-Block equation:

$$-\frac{dE}{dx} = 2\pi N_a r_e^2 m_e c^2 \rho \frac{Z}{A}\frac{z^2}{\beta^2}\left[\ln\left(\frac{2m_e \gamma\, v^2 W_{max}}{I^2}\right) - 2\beta^2 - 2\frac{C}{Z} - \delta\right]$$

The rest of the parameters are described below in Table 1:

Table 1. Parameters of Bethe-Block equation

Parameters description	Parameters description
N_a Avogadro's number.	γ Lorentz-factor
r_e Classical electron radius.	v Speed of incident Particle
m_e Atomic mass.	W_{max} Maximum energy transfer in a single collision.
c Speed of light in vacuum.	I Mean excitation potential.
ρ Density of the absorbing material.	C Shell correction.
Z Atomic number of absorbing materials.	δ Density correction.
A Atomic mass of absorbing material.	$\beta = {}^{v}/_{c}$ Relativistic velocity.
z Charge of the incident particle.	

The Bethe-Block equation describes how much the charged particle that loses energy, dE, along the done path, dx , in the medium. The formula shows how the particle projectile characteristics affect the energy loss which it is proportional to square of the charge particle and to the inverse square of velocity (Newhauser & Zhang, 2015).

2.1.2 Coulomb scattering

From the classical approach, a proton undergoes a repulsive force whilst proton passed close to the atomic nucleus makes the proton deflect from its original trajectory, this process is

called Coulomb interaction or proton-nucleus elastic scattering and it is the main mechanism interaction with the atomic nucleus (Newhauser & Zhang, 2015; Tsuboi, 2020). It is necessary to take into account this type of mechanism in dose calculation of dose distribution whether for patient or phantom with treatment planning systems (Newhauser & Zhang, 2015).

In clinical particle, Coulombe scattering plays a part in loss energy which is within 0.1% of overall energy loss (Elia, 2019). This procedure significantly recurrent elastic scattering on nuclei (Multiple Coulomb Scattering, MCS) leads to the lateral penumbra of proton beams as a function of depth, this can cause the lateral beam spread (Eric Shinohara MD, 2016, November 30; Harald Paganetti, 2018).

2.1.3 Nuclear interactions

The collision between the proton and nucleus can be elastic or non-elastic scattering, in the elastic scattering process the primary proton scattering with a large angle and the kinetic energy is conserved, the target nucleus only recoils (Breuer & Smit, 2013). In non-elastic scattering, the protons impart their energy to the target nuclei, and the target breaks apart to recoil nuclei and secondary particles, like secondary protons, neutrons, α particles, and γ rays (Tsuboi, 2020).

In the point of interaction, the recoil nuclei and the fragment are absorbed and the secondary protons are scattered large distance from the point of interaction, it contributes to a low dose, halo influence, which must take into account for dose distribution and unwanted neutrons production (Hoppe, Phillips, & Roach, 2010). Although the nuclear interaction is less frequent than proton-electron interaction and Coulomb interaction (Hoppe et al., 2010; Tsuboi, 2020), the probability of this interaction increase with the proton's energy and atomic number of the target, which in turn effects with neutrons production (Hoppe et al., 2010).

2.1 Depth Dose Curves and Dosimetry

In radiotherapy and radiation protection, a unit was placed that helped measure tissue damage caused through ionizing radiation, it is considered the precision of determining the absorbed dose key succeed major in radiotherapy treatment where help to avoid the damage to healthy tissue in case increase dose about the required limit or failure to control tumor if the dose decreases below the required limit.

2.4.1 Absorbed dose

The damage to irradiated material(tissue/organ) is measure by the energy that has been amount absorbed by it. The mean energy dE imparted and deposited to a material volume dV of specific mass dm by ionizing radiation called absorbed (physical) dose. It is defined as:

$$D = \frac{dE}{dm} = \frac{1}{\rho}\frac{dE}{dV}$$

Where ρ the density of material. Absorbed/physical dose, in the SI system uses Gray (Gy) measuring unit, where 1 Gy equal to 1 joule per kilogram (Baltas, Sakelliou, & Zamboglou, 2006).

2.4.2 Equivalent dose

Each organ and tissue have a special sensitivity to the type of radiation, which is not included in the concept of equivalent dose. The concept of equivalent dose takes into consideration each radiation type has various biological effects on tissues. It is defined as:

$$H_T = \sum_R w_R D_{T,R}$$

Where w_R represents the weighting factor for distinction radiation type set out in the Table 2, and $D_{T,R}$ is the absorbed dose over the tissue. The unit of measure is the Sievert (Sv) express as 1sv= J kg^{-1} (Charles, 2008).

Table 2. Radiation weighting factors as delimited by the International Commission on Radiological Protection (ICRP)(Charles, 2008).

Radiation types	Weighting factor, w_R
Protons and charged ions	2
Photons	1
Electrons and muons	1
Alpha particles, fission fragments and heavy ions	20
Neutrons:	
$E_n < 1MeV$	$2.5+18.2E-[\ln(E_n)]^2/6$
$1MeV \leq E_n \leq 50MeV$	$5.0+17.0E-[\ln(2E_n)]^2/6$
$E_n < 50MeV$	$2.5+3.25E-[\ln(0.004E_n)]^2/6$

2.4.3 Effective dose

Each organ and tissue have a special sensitivity to the direction of radiation which is not included in the concept of equivalent dose, the International Commission on Radiological Protection (ICRP) has been inserted the effective dose as:

$$E = \sum_T w_T H_T = \sum_T w_T \sum_R w_R D_{T,R}$$

Where w_T represent the tissue weighting factor, Table 3 classify the w_T factor(Charles, 2008).

Table 3. Tissue weighting factors(Charles, 2008).

Tissue/organ	Weighting factor, w_T
Brain, bone surface, skin, salivary glands.	0.01
Esophagus, bladder, liver, thyroid.	0.04
Gonads.	0.08
Marrow, breast, lung, bone, colon, stomach, remaining tissues (Prostate, adrenals, kidneys, extra thoracic region, gallbladder, heart, lymphatic nodes, muscle, thymus, pancreas, small intestine, spleen, uterus, cervix, and oral mucosa)	0.12

2.4.4 Isoeffective dose

The IAEA (International Atomic Energy Agency) and ICRU took addition factors into consideration for combined or compared various types of treatment, and insert the isoeffective absorbed dose, D_{IosE}, concept. isoeffective absorbed dose is the dose the conveyed undergoing the reference conditions, for instance (photon, 2Gy/fr, 5fr/week), to produce the very effects like the actual treatment $D_{IosE} = D \times W_{IosE}$.

D the total delivered dose, W_{IosE} weighting factor, which considers all factors (biological effects, RBE, LET, dose per fraction, dose rate α/β). In proton therapy a generic RBE=1.1 is applied instead of W_{IosE} and become $D_{IosE} = D \times 1.1$, this expression called an RBE-weighted dose (the product of RBE=1.1 and the physical dose), units of biological dose Gy(RBE) which takes into consideration the biological effectiveness of the radiation type. The Figure 6 shows

the variants in the depth-dose curve of physical/absorbed dose VS bio-effective/isoeffective dose (Andre Wambersie et al., 2006; André Wambersie et al., 2011).

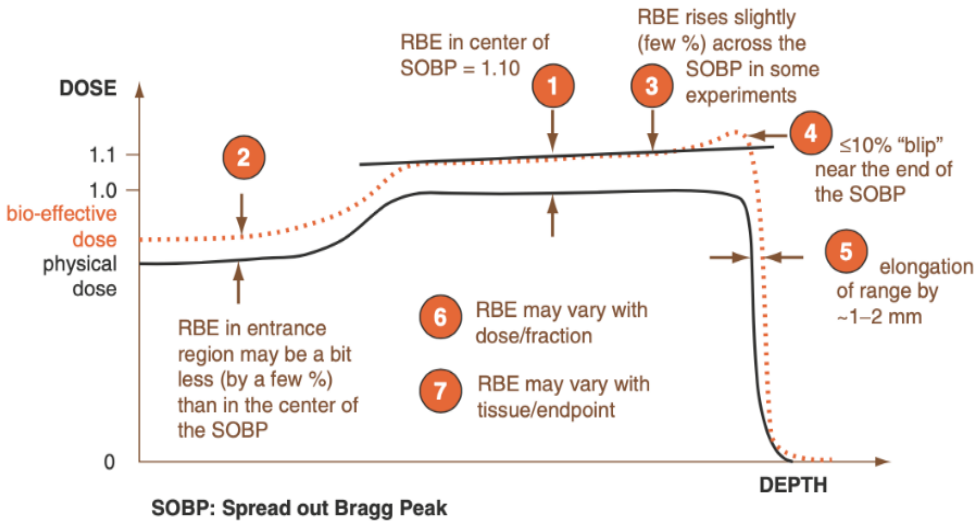

Figure 6. The solid line represents the physical dose and the dotted line represents bio-effective dose/RBE-weighted dose corresponding dose weighted for radiation quality (RBE=1.1) (Beahrs & Henson, 1992).

Relative biological effectiveness, RBE, in proton therapy has been based on the use of generic RBE of 1.1 within tumors and normal tissues, ignoring the generic value RBE=1.1, not constant, and it is dissimilar on this value as Figure 6 shows since RBE depends on factors as mention above, by the article of Paganetti found the RBE =1.1 at the entrance of beam and RBE=1.3, RBE=1.7 at the distal edge and distal fall-off region respectively, the RBE value increases at the distal range of proton beam which leads to increase the biological effect in the distal range of the dose deposition and it corresponding to the energy decreases. This effect can be express by the concept of the RBE-weighted dose, where reference to the product of the RBE and physical dose. (Anferov & Das, 2015; Harald Paganetti, 2003; Harald Paganetti et al., 2002).

2.4.5 Spread-out Bragg peak and dose deposition

In Figure 7, shows the difference in the way deposited dose of protons compared to the dose of photons in the target (tumor). For protons, the dose is low at the entrance and increases until the longitudinally narrow Bragg peak is reached (Mono-energetic and Multi-energetic proton state), followed by trivial dose distal fall-off beyond the Bragg peak with avoiding healthy tissue for the dose and it does not suitable for treatment to volume target whole, instead of that uses the concept of spread-out Bragg peak to cover the required target. For photons, the largest dose deposited in near-surface tissue, and even after the traversing target deposit a few unfavorable doses conversely of protons dose (Harald Paganetti, 2018).

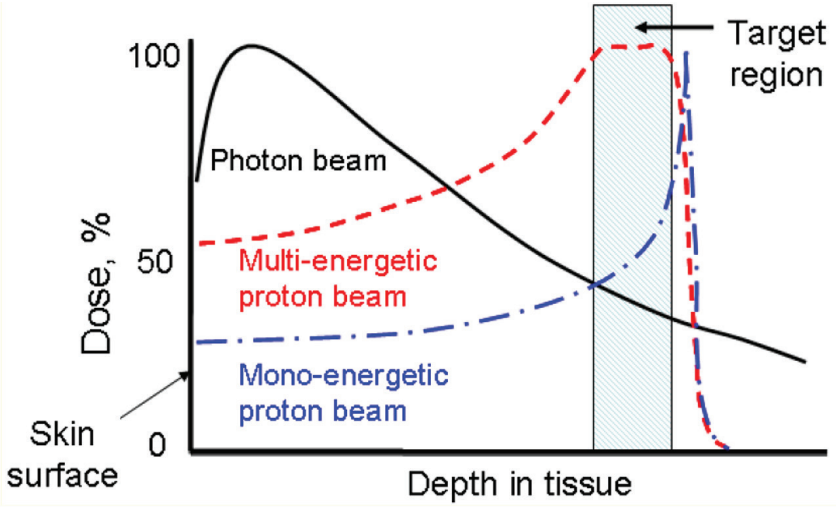

Figure 7. Illustration of depth-dose curves for proton, photon, and SOBP beam (Zhu & Yoon, 2013).

2.3 Radiation Biology

The ability of ionization radiation to kill and destroy cancer cells without surgical intervention aroused widespread interest in the medical community. Destruction of a cell's

DNA completely is the certain cell death and an inability to proliferate, the ionization radiation has the ability to two different damage direct and indirect action (damage) types to DNA. Charged particles are capable of either direct damage of DNA by a single-strand break (SSB) or a double-strand break (DSB) as Figure 8 illustrates. Through SSB the cell's DNA can be repaired easily contrary to a DSB where DNA is unable repair and be harder to proliferate. The SSB type can have same impact as DSB if damage site occurs near short distance of each other. The other capability is indirect damage by producing free radicals across reaction with the water within the cell and it caused damage to adjacent DNA. Approximately 70 % of the proton energy loss be moved up delta-electron production and may be able to contribute to ionizing which lead to further strand breaks DNA. The indirect damage dominates through a low LET value and as a LET value increases the direct damage influence becomes conspicuous(Baskar, Dai, Wenlong, Yeo, & Yeoh, 2014).

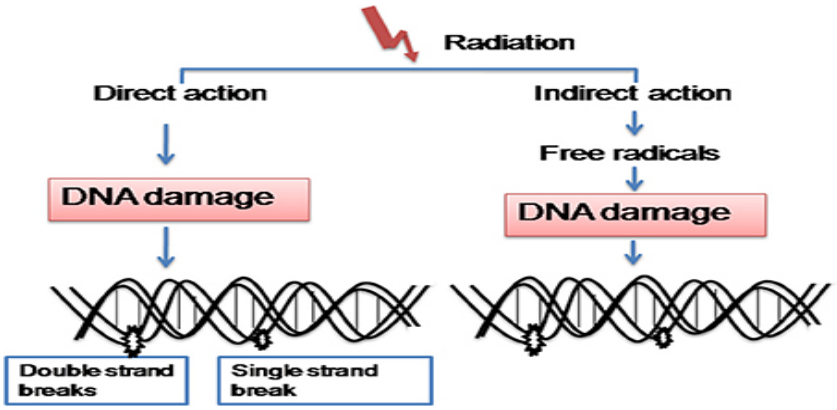

Figure 8. Radiation process of direct/indirect action (Baskar et al., 2014).

2.3.1 The Linear-Quadratic model

The linear-quadratic model is part of important tools in radiobiology, it describes the relationship between the delivery dose and the promotions of cells that survive in accordance with the following formula:

$$s = e^{-\alpha D} + e^{-\beta D^2}$$

Where S is the cell survival, D represents the exposure dose and α and β represents the linear and quadratic parameters respectively, and these describing the cell's radiosensitivity. Through cell survival plotted on a log scale it gives a quadratic response curve as a function of dose as depicted in the figure 9. This shows the two components to cell killing, α D-cell killing (irreparable-cell) and β D^2-cell killing (reparable-cell) combine to form a cell survival curve.

α / β ratio is the dose at which log surviving for α D linear-component and β D^2 quadratic-component of cell killing are equal and it depends on radiation tissue type, for the specific tissues represents the ratio of essential radiosensitivity for it to repair capability, is given in Gy unit. Tumors and early responding tissue usually have a high α / β value between 7~10 Gy, and late responding normal tissue usually have α / β value from 3 to 5 Gy. As Figure 9 shows, the late responding tissue is more curved than early responding tissue and this leads for the survival fraction reduces more greatly as the dose heightens(Balagamwala, Chao, & Suh, 2012).

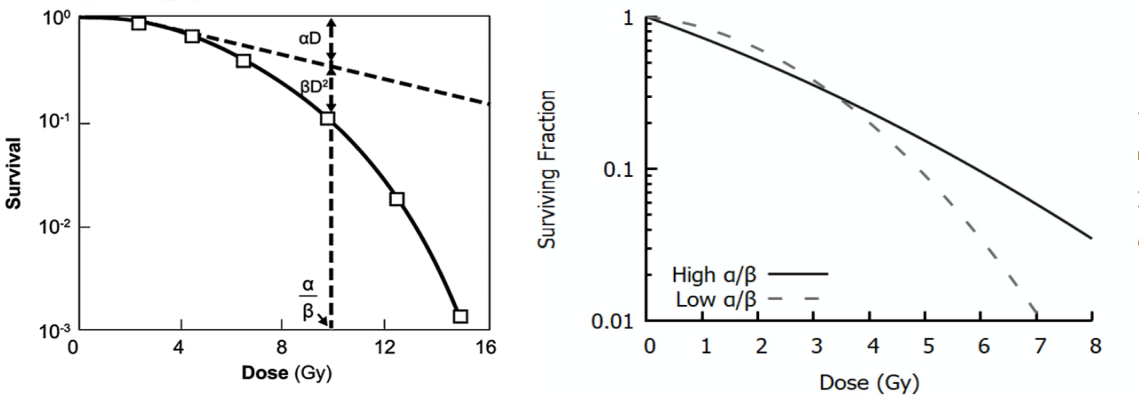

Figure 9. On the left side the survival curve for linear and quadratic components and the displays of α / β ratio point, on the right side the survival for high and low α / β ratio (Balagamwala et al., 2012; McMahon, 2018).

2.3.2 Linear energy transfer and analytical models

The side effects of radiation impact the quality of life of patients treated with radiotherapy and lead to normal tissue complications. The concept of linear energy transfer includes the perception of potential biological damage to the target through one of the radiation types used in radiotherapy.

The irradiation causes biological cell damage proportional to the deposited energy of radiation in the target. The biological effects of ionizing radiation rely on some factors like the kind and size of the target and the radiation properties, for the same energy, heavy particles (alpha particles, proton, and neutron) deposit their energy for a much shorter distance than gamma rays and X-rays. The linear energy transfer is proportional to the velocity and the charge of ionizing radiation; accordingly, it increases the charge velocity (kinetic energy) decrease and as the charge of ionizing radiation increases as illustrated in Figure 4 and 2, this corresponds to lethal effects and the relative biological effectiveness (RBE) increase as the LET increase, look over at Figure 5. At the same time, at the distal-off dose corresponding to a high value of LET as Figure 10 shows. Table 2 below shows LET values for different radiations types (Beyzadeoglu, Ozyigit, & Ebruli, 2010).

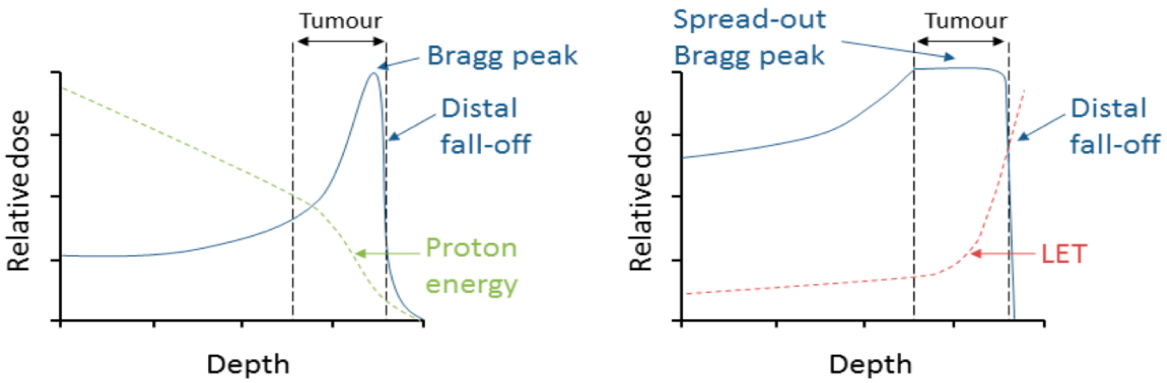

Figure 10. Proton depth dose distribution and relation of LET and proton energy (Vitti & Parsons, 2019).

Radiation	Energy	Relative LET value (keV/μm)
250 kV X-ray	250 kV	3
3 MV X-ray	3 MV	0.3
Cobalt 60	1.17–133 MV	0.3
Beta 10 kV	10 kV	2.3
Beta 1 MV	1 MV	0.25
Neutron 2.5 MV	2.5 MV	20
Neutron 19 MV	19 MV	7
Proton 2 MV	2 MV	16
Alpha 5 MV	5 MV	100

Table 4.LET values for different radiations types (Beyzadeoglu et al., 2010).

The charged particles lose energy as they traveling through the medium by inelastic interaction with atomic electrons as described by Bethe-Bloch formula. Zirkle described the absorbed energy by the medium as the linear energy transfer (Zirkle, Marchbank, & Kuck, 1951), LET, of charged particles measures the energy absorbed (dE) by medium per unit path length (dx). It can be written as:

$$\mathrm{LET} = \frac{\mathrm{dE}}{\mathrm{dx}} \ (\mathrm{keV/\mu m})$$

It used to quantify the effects of ionizing radiation on biological samples (Breuer & Smit, 2013). High-LET deposit more amount energy per unit path of the target more than the same dose of low-LET (which deposit less amount of energy) high-LET cause significant DNA damage (Beyzadeoglu et al., 2012). It considered low-LET radiation when the LET below 10 keV/μm, while above 10 keV/μm is regarded as high-LET radiation (Park & Kang, 2011).

Actually, the concept of LET is a similar description of the stopping power,S, the exclusion of the effects of radiative energy loss, for instance, Bremsstrahlung or δ -rays (Park & Kang, 2011). The linear energy transfer is defined by ICRU report 90 as the restricted LET ("Report 90," 2016) by:

$$L_{\Delta} = \frac{dE_{\Delta}}{dx} = S_{el} - \frac{dE_{Ke,\Delta}}{dx}$$

Where dE_{Δ} the energy lost by charge particle due to inelastic interaction with atomic electrons minus the aggregate of kinetic energy for electrons liberated with kinetic energy $dE_{Ke,\Delta} > \Delta$ by charged particles over a track, dx , and S_{el} refer to linear stopping power (Baltas et al., 2006). Δ represents energy cut-off, expressed by eV, not range cut-off although the restricted linear energy transfer represents the energy loss locally imparted (Units, 1998).

The LET called unrestricted energy transfer, L_{∞}, in case contains δ -rays and all electronic interactions and ignored the energy cut-off, then $L_{\infty} = S_{el}$ and it is equal to electronic stopping power concept and been used to calculate the absorbed dose for this case, as shown in Figure 2, displays the relation between the LET of protons and the kinetic energy of proton (Tsuboi, 2020).

The calculation of LET is easily reached in regard to monochromic beams due to the clearly defined kinetic energy, there various considerations that are needed for non-mon-energetic in which calculation of L_{∞} shows more complex (Wilkens & Oelfke, 2003).

Protons in the substance are subject to Coulomb interaction and nonelastic nuclear interaction, the non-elastic nuclear interaction takes place frequently in the entryway of the Bragg curve and the value of LET tends to be small and slightly different. The commonest interaction process is the Coulomb interactions of primary protons are considered and it takes this into consideration for an analytical LET model, mostly at the distal edge and around the crest of Bragg curve which corresponds to an increase of LET, the absorbed dose is affected through this interaction. The dose behind the Bragg peak which come from secondary particle can be neglected (H Paganetti, 2002; Wilkens & Oelfke, 2003).

The international commission on radiation units and measurement (ICRU) introduce two different concepts of LET to the track-average LETt (the track divides into equal length and the energy average deposited in each length), and the dose-average, LETd (the track divides into equal energy and averaging the track length deposited these energy in the track length) ("Report 16," 2016). The dose-average, LETd, has become of regard in use into the treatment planning system and biologically effects (Grassberger & Paganetti, 2011). The LETt defined as the mean value, arithmetic average, S for all protons weighted by fluence, while the LETd for every single proton is weighted by it is contributions to the local dose. In order to figure a mean of LET for every kind of particle independently, utilizes the stopping power and energy spectrum then take the total of their average to get total LET (Wilkens & Oelfke, 2003). Both of LETt and LETd depend on the local energy spectrum at the point/place x. It can describe the spectrum with reference to residual range of particle by the concept of the continuous-slowing-down approximation (CSDA) which gives the relation between the residual range and the energy, therefore LET_t at the point x is given by:

$$LETt(x) = \frac{\int_0^\infty \varphi_r(x)S(r)dr}{\int_0^\infty \varphi_r(x)dr}$$

where r indicates to the residual range at the point x, $\varphi_r(x)$ the local particle spectrum at the point x, $S(r)$ the stopping power of primary protons into residual range r and, $\varphi_r(x)dr$ represent the fluence of protons at the point x with residual range within r and $r + dr$.

Similarly, the LET_d is given by:

$$LETd(x) = \frac{\int_0^\infty \varphi_r(x)S^2(r)dr}{\int_0^\infty \varphi_r(x)S(r)dr}$$

In the case of the monoenergetic protons, both LETd and LETt equivalent the stopping power S. The equations above for, LETd and LETt represent for single beam of proton, for n beams with the local fluence spectra $\varphi_{r,j}(x)$ at the point x, the track averaged, LETt, and the dose average, LETt, become (Wilkens & Oelfke, 2003):

$$\mathrm{LETt}(x) = \frac{\sum_{j=1}^{n} \int_0^{\infty} \varphi_{r,j}(x) S(r) dr}{\sum_{j=1}^{n} \int_0^{\infty} \varphi_{r,j}(x) dr}$$

and

$$\mathrm{LETd}(x) = \frac{\sum_{j=1}^{n} \int_0^{\infty} \varphi_{r,j}(x) S^2(r) dr}{\sum_{j=1}^{n} \int_0^{\infty} \varphi_{r,j}(x) S(r) dr}$$

2.3.3 Relative biological effectiveness

Relative biological effectiveness, RBE, is determined as the ratio between standard radiation dose, X-rays or gamma-rays, to the test radiation dose to cause the same biological effect goals, it is evaluating or/and compares the biological effect of a specific type of radiation with a standard radiation. In proton therapy, all treatments are performed with an RBE of 1.1 without regard to depth in the tissue, cell kinds, dose per fraction, dose rate and biological endpoint, this presumption was determined from past experimental data basically gotten at the middle of SOBP. RBE is a complicated conception to match the standard radiation with the test radiation in the same circumstances due to the RBE relies on many factors such as dose per fractions, LET, cell kinds, endpoint, exposure conditions, and the energy of particles.

Experiments indicated that LET and RBE are exceedingly related, where the latter increasing as LET be increasing in certain limits, it has been observed RBE values decrease at LET

surpassed 100 keV/ μ m. Beyond this LET value, the RBE inclines because of cell overkill. This is due to high LET particles densely ionization executed on the cell, DNA, that is required for DNA damage. Proton particles impact to clustered DNA damage more than photons. As the Figure 11 shows this tenor(Willers et al., 2018).

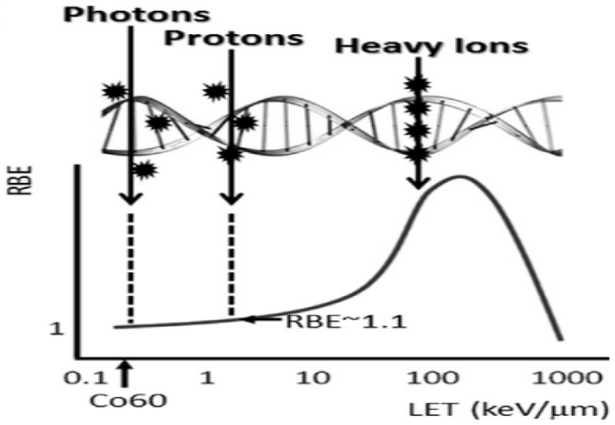

Figure 11. Illustration of positive relationship of RBE and LET, and shows how protons product of cluster DNA damage cluster compared to photons (Willers et al., 2018).

3. Patient Data and Treatment Planning

Treatment planning systems (TPS) are the core of the radiation therapy (RT) systems, and the tool to enhanced patient upshots, through patient images and identified the tumour, TPS construct an integral plan for each beam track to deliver the treatment, dose, to the tumour appropriately.

The primary challenge is to form a plan delivered high dose to the tumour conveniently and minimize the healthy tissue and organs at risk of high dose radiation concurrently, there are several systems in use the treatment planning systems, for instance, Brainlab, Elekta, Philips, Prowess, Raysearch and Varian Eclipse, the latter is used in this thesis (FORNELL, July, 2013).

3.1 Digital Image Acquisition

The treatment planning requires the patient's images to be of high accuracy and taken correctly according to the patient's position in order to make it possible to estimate the location and dimensions of the tumour additionally to potential organs at risk, in addition to helping to obtain information about tissue density that helps to make accurate calculations of dose distribution.

The medical imaging modalities utilized are several and variety like positron emission tomography (PET), ultrasound (US), magnetic resonance imaging (MRI), and computed tomography (CT). The CT provides tissue density information and represents the gold standard in radiotherapy (Khan & Gibbons, 2014).

The computed tomography (CT) scan consists of a series of X-ray images extracted from a different angle, in which X-rays are geared toward and rapidly rotated continuously at the body patient in a helical shape called a gantry, the X-rays exits of the patient body and

capture by detectors, the machine's computer processes the signals come from the detectors and assists to create cross-sectional images (slices), as soon as several successive slices are collected by the machine's computer simultaneously it lead to form a three-dimensional image of the patient and allows to designation the location of basic structures in addition to potential tumours(Smith & Webb, 2010). The principle of CT is based on the intensity of photons penetrating medium can be calculated by the equation:

$$I = I_0 e^{-\mu x}$$

Where I is the amount of photon intensity after crossing the medium, I_0 is the primary photon intensity, μ is the linear attenuation coefficient which represents the number of photons absorbed per cm, and x is the thickness of the absorbing medium. The attenuation coefficient relies on the density of penetrate the medium. Therefore, the grayscale is used in X-ray images to describe the different attenuation according to the attenuation scale, in which the darker areas on the X-ray image correspond at occurred less attenuation on low relative density regions, at the high relative density where highly attenuation the brighter areas appear (Khan & Gibbons, 2014).

3.2 The Hounsfield Unit

The grayscale CT images as it appears in the figure were placed by using the Hounsfield Unit (HU) also called CT number to regions has variant attenuation of radiation as show in Figure 12, the HU is calculated based on a linear transformation of the linear attenuation coefficient of the X-ray and defined as:

$$HU = 1000 \times \frac{\mu_{tissue} - \mu_{water}}{\mu_{water}}$$

Where, water is defined to have $HU = 0$, $HU = 1000$ to dense bone and $HU = -1000$ to air, the linear transformation produces a HU scale that displays grayscale. In order of maximal photons absorption in more dense tissue, the HU has positive values and seems bright, with regard to minimal photons absorption in less dense tissue, the HU has negative values and seems dark. In proton therapy, the range of protons can be calculating by converted the HU into relative stopping power values(Ainsley & Yeager, 2014).

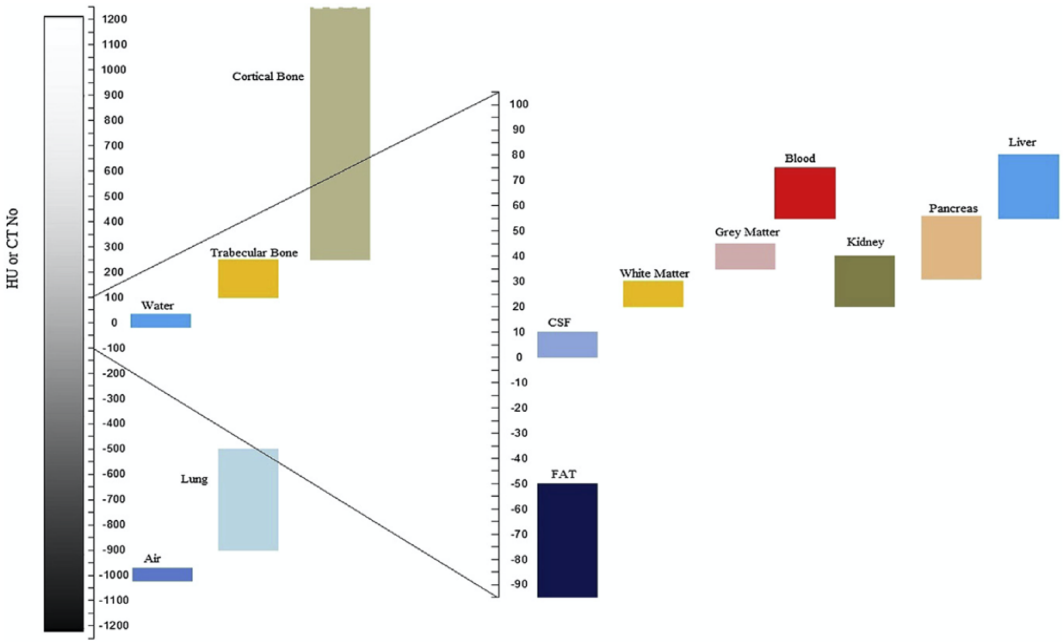

Figure 12. Hounsfield number for various human tissues (Kalra, 2018).

3.3 Volumetric and Target Delineation

The development in computer technology during recent decades, which helped in the possibility of planning the dose of radiation therapy in three dimensions and radiotherapy treatment, leads to the need to insert specific definitions for each tumor and the areas of potential spread were presuppose. According to the methods mentioned above to get patient's image, each of the targets and volumes utilized to treatment by radiation therapy had been defined in ICRU Report 50(D. Jones, 1994).

3.3.1 Gross tumor volume (GTV)

GTV is defined as a visible/palpable tumor by imaging the tumor using modern diagnostic imaging modalities such as PET, MRI, or CT, the GTV be formed of the primary tumor and high cell density and therefore sufficient dose must constantly be delivered to the whole volume for therapy(Harald Paganetti, 2018).

3.3.2 Clinical target volume (CTV)

The GTV is just not the main malignant region only, often includes extends from the main malignant in the form of individual malignant cells or small malignant cell bunch that is hard to be clinically noticed. So, the CTV included the GTV region in addition to these extended tumor cells(Harald Paganetti, 2018).

3.3.3 Planning target volume (PTV)

Once the entire macroscopic tumor became delineated, must be taken into account the patient movement or placement of the malignant cells on the nearness of the organ motion for instance lungs and heart. To guarantee the suitable treatment of the whole CTV. The planning target volume (PTV) can extend beyond CTV and takes such potential problems into account by adding a margin of these considerations around the CTV. The PTV is used for handling dose prescriptions to guarantee delivery of the prescribed dose to the whole CTV(Barrett, Morris, Dobbs, & Roques, 2009; Harald Paganetti, 2018).

3.3.4 Organ at risk (OAR)

Once making radiation treatment of a patient, the treatment planning should be included the organs where have sensitive to radiation that they can greatly impact the treatment planning

or the prescribed dose, these sensitive organs should be delineated and be called organs at risk (OAR)(Tsuboi, Sakae, & Gerelchuluun, 2020). Figure 13 below illustration the delineated of these various target volumes.

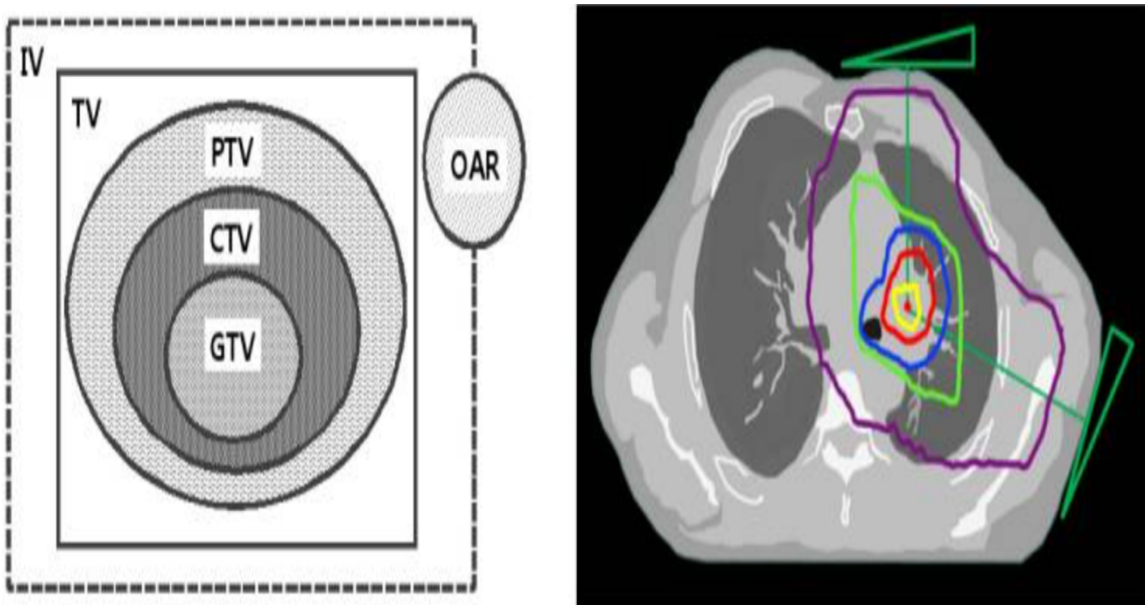

Figure 13. The right side represents lung cancer radiotherapy and the sketch of the left side the treatment volumes where, irradiation volume (IV-purple), treated volume (TV-green), planning target volume (PTV-blue), clinical target volume (CTV-red), gross tumor volume (GTV-yellow) and organs at risk(OAR)(Hyun Mi Kim, 2018, Feb).

3.4 Plan Assessment of Radiotherapy

The objective of radiotherapy is to deliver the appropriate dose to the target and avoid the normal tissue and organ at risk. Ways of estimating the treatment plan can be achieved through different methods. The dose distribution and volumetric are analyzed and examined using dose distribution showing and dose-volume histograms.

3.4.1 Dose-volume histograms

Dose-volume histograms (DVH) relates dose of radiation to tissue and/or organ volume in treatment planning as a histogram. The DVHs are mostly widely utilizing to put it briefly the

simulated dose distribution inside a volume of interest of a patient which would result from a suggested treatment plan and/or to compare doses from various plans. (Drzymala et al., 1991).

3.4.2 Dose distributions

The dose distribution may become optically examined utilizing color wash added on the CT images. The color wash displays the dose distribution color bar clearly defined, where generally the cooler colors describe the lower dose, and the warmer colors describe the higher dose. Whereas the presence of dose accordance with the color wash form over the CT images gives an easy and logical impression of how the dose is dispersed, it tends to be hard to appropriately assess treatment plans as far as the measure of dose organs and targets that irradiated(Brady, Heilmann, & Molls, 2006).

3.5 Treatment Delivery and Accelerators

3.5.1 Accelerators and energy modulation

In particle radiotherapy usually utilized accelerators to achieve the energy of particle required. In proton therapy, the two main types of accelerators; the cyclotron and the synchrotron. An energy required for radiation depth of 30 cm in tissue by protons about 230-250 MeV using the accelerators mentioned above. A cyclotron consists of a pair metal flat of semicircular shape called 'Dees'; the particle charged source (source of ions) injected among the center of the gap between two Dees. Under high-frequency alternating voltage and magnetic field, the particles are accelerated in an outward from the center along a spiral path until they reach the as much energy allowed by the cyclotron, at that moment they are extracted. However, one limitation of the cyclotron does not operate when charge particles gain extremely high speeds, the mass increasing as the speed increasing and this leads the charge particle take long time to complete the semicircular track inside the dee, it is unable to accelerate these particles further, so

synchrotron comes that can accelerate charged particles beyond a relativistic speed and not suited for ions heavier than protons. The advantage of a cyclotron is the ability to produce a continuous beam of particles, where is unable to execute by a synchrotron. In return, the disadvantage of a cyclotron is the fixed energy of accelerator particles required. Cyclotrons can accelerate protons until the energy range of 230-250 MeV and by using energy modulation to achieve lower energies through degrader as against the beam after extracting or inside the treatment nozzle itself, this called passive-modulation(Brady et al., 2006; Coutrakon, 2007).

A synchrotron is considering large machine compared to the cyclotron, using a linear accelerator for charged particles before entering the synchrotron, the synchrotron made-up of a circular form of a long-evacuated tube with robust magnets utilized for bending the particle charged path and for focus the beam. The energies at which the particles are accelerated can be changed within the accelerator by controlling the magnetic field strength, which is called active-modulation. The illustrations show a simplified schematic of 14(a) synchrotron and 14(b)cyclotron.

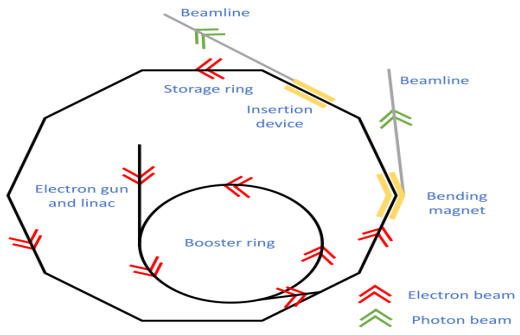

Figure 14(a). Simplified schematic of synchrotron (Godfrey, 2018).

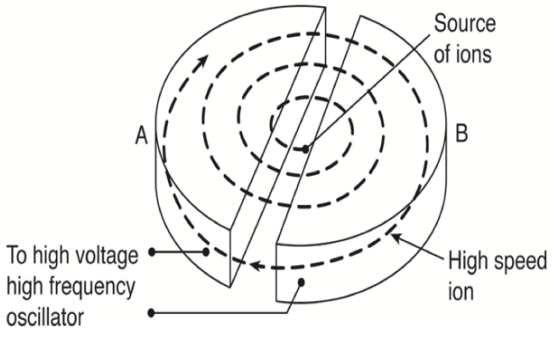

Figure 14(b). Simplified schematic of cyclotron (Coutrakon, 2007).

3.5.2 Techniques of beam delivery

The aim of particle therapy is the dose to be conformed to the destination volume, a monoenergetic beam give longitudinal tiny Bragg peak where is unhelpful in the treatment, the active and passive modalities mentioned above spread the beam to the destination volume in the longitudinal direction(depth-dose), to fill the whole target volume in the lateral direction, there are two methods have been using in order to spread the beam are names the pencil beam scanning (PBS) and passive scattering (PS) (Mayles, Nahum, & Rosenwald, 2007).

Passive Scattering

Passive scattering (PS) is considered an old technique particle therapy, to achieve of lateral direction of the narrow particle beam according to the lateral dimension which required, usually by using a single scattering with one scatter foil in order to small field are or by double scattering through using two scatter foils, the treatment beam can be formed based on the target volume required using a tool called collimators to use for each individual treatment beam. The collimation tool may take place an additional dose to the patient due to the interaction properties of the collimator material with the treatment beam via secondary radiations, which gives the disadvantage to the passive scattering technique(Mayles et al., 2007). In Figure 15a shows the passive scattering techniques details.

Pencil Beam Scanning

Pencil beam scanning (PBS) or as called scanning beam is the most precise in proton therapy treatment. PBS is involved sending a narrow proton beam through utilized a pair of magnetic dipoles of the X-axis and Y-axis to handle deflect and distributing the beam directly to the target volume as required in the lateral direction and can achieve various depths of

dose deposition by altering of the energy where enable control of dose distribution without the assistance of passive components and that leads no additional dose to which result comes from secondaries radiation. Consequently, the target volume can be scanned by the beam each slice of the target separately. The beam scanned kind determines according to the irradiation treatment demand for one layer of voxels or in order to each voxel separately. The Pencil beam scanning can be dose conform for the proximal and distal end of the target therapy helps to avoid the high doses to normal tissue which is an advantage for PBS(Mayles et al., 2007). Pencil beam scanning is shown in Figure 15b.

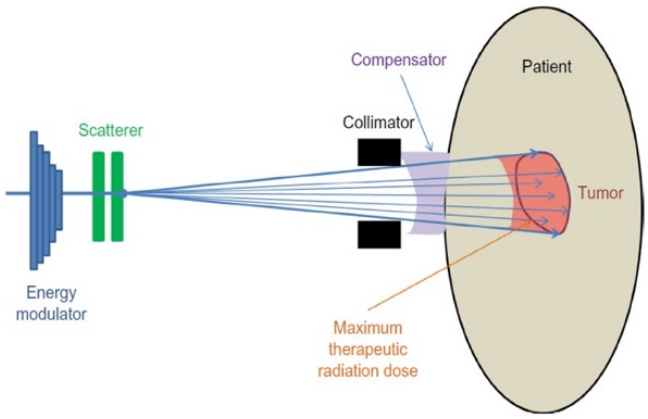

Figure 15a. Illustration of the passive scattering (Wang, 2015).

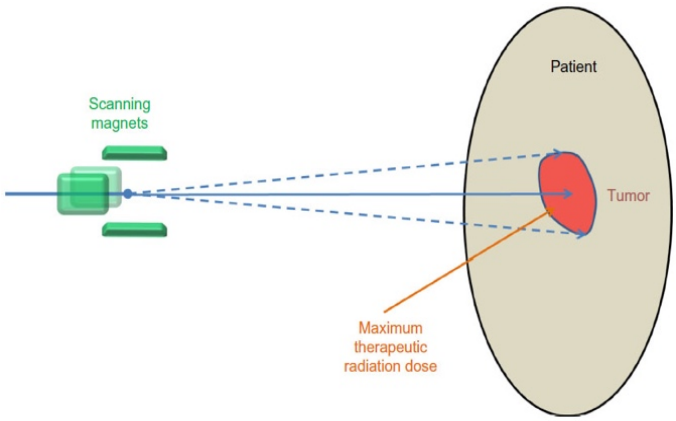

Figure 15b. Illustration of the pencil beam scanning (Wang, 2015).

4. Simulations of Dose and LET

The information technology makes a great contribution in therapeutic and diagnostic applications of ionizing radiation (Grassberger & Paganetti, 2011). The Monte Carlo, MC, technique has become omnipresent in medical physics in recent decades because of increase interested of particle interaction and transport in the medium and help of dosimetric calculation in radiation therapy from internal dosimetry of nuclear therapy and help to the treatment planning in external radiation to estimate the distribution of radiation dose in contrastive medium e.g. lung and bone (Amato, Lizio, & Baldari, 2013; Verburg et al., 2016). In proton therapy, many Monte Carlo codes are used, for instance, Geant4, FLUKA, EGS, and MCNP, these codes vary in accuracy small difference in the user interface, and vary in grade of control onto tracking parameters (Amato et al., 2013; Seco & Verhaegen, 2013). MC simulation is utilized to model the probability of various results in a process that difficult to predict due to the interference of random variables. It is a procedure used to understand the effect of risk and uncertainty in prediction models, and also gives a thought of what results to expect as well as the likelihood of the event of that result. This feature made a lot of fields and branches to use MC simulation like physics, statistics, and finance (Amato et al., 2013).

4.1 FLUKA

FLUKA is one of MC code (Böhlen et al., 2014) and is a multipurpose in numerous fields, and capable of study 60 various particles, which be good consider to simulate for electromagnetic and hadron particle interaction and transport in any target through a broad energy domain (Ferrari, Sala, Fasso, & Ranft, 2014). The electromagnet and muon interaction can be simulated up to 100 TeV, the hadron interactions up to 100 TeV. The code has the potential to track particles in the magnetic and electric field and simulate the

optical photons (Giuseppe Battistoni et al., 2011). The graphical user interface, called Flair, supports to use for FLUKA Monte Carlo code (Ferrari et al., 2014). FLUKA depends on original and all-around tried microscope models. Improves consequence FLUKA model performance and make it more realistic and accurate through comparing with experimental particle production data at single interaction levels (Giuseppe Battistoni et al., 2011).

4.2 Eclipse

The Eclipse treatment planning system, Eclipse (TPS), is a treatment planning software utilized to plan external beam irradiation with photon, proton and electron beam. Since the treatment therapy system generally contains beam production region, delivery beamline system, and treatment machine area (nozzle), Eclipse binds between the treatment machine and a treatment planning system and gains information used for treatment planning from the patient's CT image and from the compared databases at treatment machine at site. It includes a variety of treatment templates that help simplify the process of creating customized treatment plans for each patient and that to save time instead of building a plan from the starting point, where the Eclipse enables the specialist to modify formerly set up treatment according to a requirement of treatment. The three-dimensional dose calculation algorithm upholds for passive scattering and pencil beam scanning both(Varian, 2015).

5. Methods

The main purpose of this project was to calculate the LETd for water phantoms and patients by using both the FLUKA MC code combined with in-house scripts from our research group (Fjæra, 2016) and the Eclipse prototype estimator for LET which uses an analytical LET calculation script which is integrated into the Eclipse software. An additional aim was to compare the LETd from the two methods in terms of LET volume histograms and LET metrics as well as colorwash plots of LETd distributions in the phantoms and patients. In the final phase of the project, RBE-weighted doses (biological dose) were also calculated to estimate the impact of different LET calculations on the final estimated RBE-weighted dose.

The data of the treatment planning system are sorted as DICOM file format and was extracted from existing treatment plans and translated for simulations in FLUKA and further analyses and visualized utilizing Python (v2.7) programming language and the Slicer software (v4.11.0), a software platform used for visualization and medical image computing. Python was used to visualize two-dimensional dose and LET distributions while Slicer was used to plot Dose-volume histograms.

5.1 Simulation Process of Water-Phantom dose plans

The water phantom plan and dose distributions were generated in the Eclipse treatment planning system for proton therapy. The water phantom was a 30 x 30 x 30 cm^3 water volume, with a 4 x 4 x 4 cm^3 target volume (PTV) located in the center of the phantom. The plan consists of two opposing proton beam fields with energies ranging from 103 to 132 MeV, and a dose prescription of 2 Gy (RBE1.1) to the PTV. The simulations were executed using the proceedings shown in Figure 16 and described in detail in section 5.3.

5.2 Simulation Process of the Patient Treatment Plan

A brain tumour case was applied, with a treatment plan and dose distributions created in the Eclipse treatment planning system for proton therapy at Haukeland University Hospital. The plan composes of two opposing fields, where the beam energies of the first field had a range of 70-125 MeV with a gantry angle of 270^0 and the second field had energies ranging from 81 MeV to 131 MeV with a 90^0 gantry angle. The total number of protons for two fields combined was 1.29×10^{12}. The plan had a prescribed dose of 54 Gy (RBE) to the PTV, delivered in 30 fractions.

Figure 16 shows the steps that have been done to execute the FLUKA simulations and additional scripts, according to the process created from our research group (Fjæra, 2016). These steps are described in the following paragraphs.

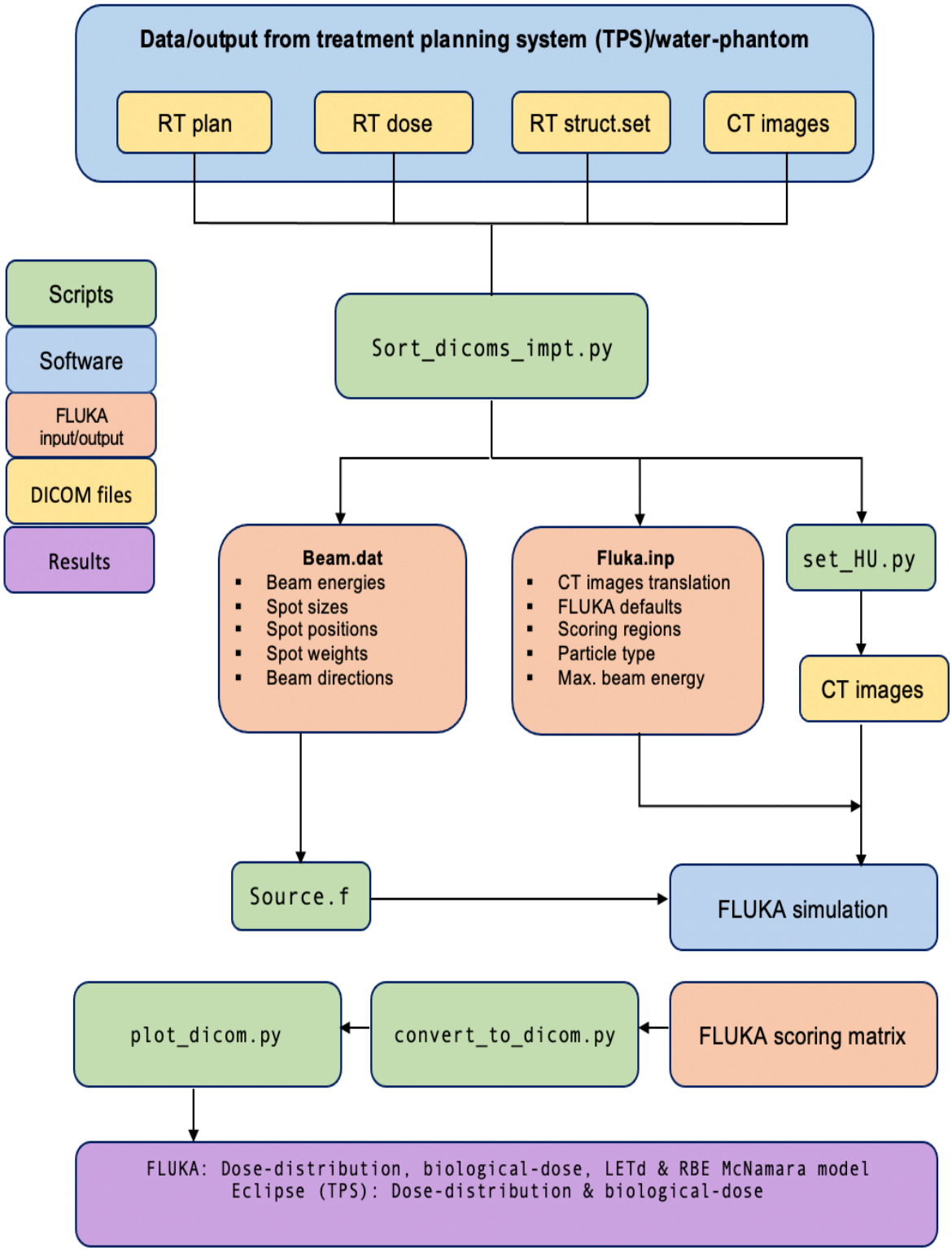

Figure 16. Illustration for implementing patient treatment plans in FLUKA MC recalculation simulations (Fjæra, 2016).

The FLUKA recalculation scripts are used to recalculate treatment plans from the Eclipse TPS at the Haukeland University Hospital bound in Bergen for IMPT. In addition to enable Monte Carlo simulations, these scripts can be used to plot dose-volume histograms, compare dose, RBE, and LET. These scripts were in this project used together with the FLUKA version (v.2011.2c.4) and the FLUKA graphical interface Flair (version 2.3), both operated by Unix based systems (Mac OS and Linux). The FLUKA simulation recalculation was enabled and done by using the scripts as described in the following sections.

5.3 DICOM File Handling and Generation of FLUKA Input File

After a treatment planning system has been applied to calculate and evaluate a treatment plan, the DICOM files (yellow boxes in Figure 16) containing the treatment information, including the dose profiles, structures, and patient images, were exported through the script called Sort_dicoms_impt.py. This script was used to build the files that are needed for the FLUKA recalculation of dose and LET. This script creates the environment necessary for executing recalculations, in simple terms, the DICOM files that the user got from Eclipse-IMPT-plan has been sorted inside a folder which includes some files needed to recalculate each single treatment plan separately:

- CT images of patient.
- RT Structure – Coordinates and colors of delineated structures
- RT Plan – details of the treatment plan itself for example proton beam spots, gantry angle.
- RT Dose – Includes information regarding the delivered dose to the patient, Where the user has single file of RT Dose for each treatment field separately, and one file for all treatment fields combined.

At same time, this script creates files used it in the input of FLUKA recalculation, these data concerning about:

- Maximum number of regions in FLUKA– 5000.
- Source routine card needed for source.f routine which defines the primary beam properties
- Physics settings HADROTHErapy (described below).
- Momentum spread for General Cap Machine in Eclipse at Haukeland – 0.9%.
- Voxel card containing the patient position in the FLUKA coordinate system.
- USERWEIGH card needed for fluscw.f routine which is used for dose and LET scoring

- Scoring cards, where bin 40, 41 and 50 has been used and based on the fluscw.f routine (the primary Monte Carlo tools calculate dose-to-material and fluscw.f routine used to calculate dose-to-water) and all LET are the unrestricted LET,L_∞,in water where:
- Bin-50 represents deposited of Dose-to-water from all particles (LET × fluence).
- Bin-40 represents deposited of Dose-to-water from all protons only (LET × fluence).
- Bin-41 represents deposited of Dose-to-water from all protons only from all protons only multiplied with electronic stopping power, $L_\infty = S_{el}$,(LET^2 × fluence). as Figure 17 shows below.
- a .dat file is generated and contains information (beam directions and energies, spot size, etc) of per pencil beam that had been used for a single treatment field.

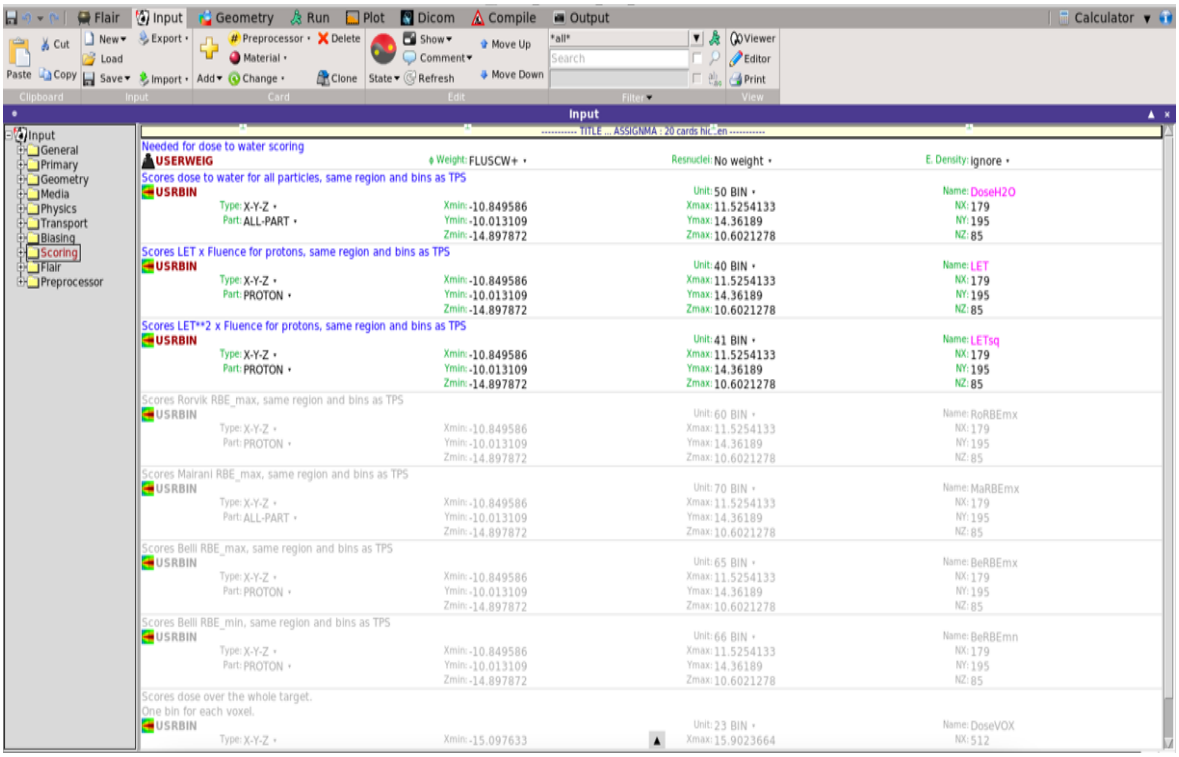

Figure 17. illustrations of BIN and USERWEIG card on FLAIR.

5.4 Setting HU Units

The script set_HU.py was operated and used to set a Hounsfield unit of -1024, which represents vacuum, outside the patient (for consistency with the TPS dose calculations) in the CT images. The CT images were then used to generate a voxel file(.vxl), which gives information of the CT in FLUKA.

5.5 Running the Simulation

5.5.1 DEAFULTS card

Prior to the initiation FLUKA simulation, FLUKA gives a category of default physics settings miscellaneous, helping the user to select and choose the appropriate setting for particular applications and in turn to define what FLUKA appropriate defaults to be utilized for recalculation condition. In this project the HADROTHErapy DEAFULTS card has been used for water phantom plan simulation and patient treatment plan simulation shows in the Figure 18, as this is recommended for particle therapy applications. Functions framework of this kind of card are:

- Δ-ray production on with threshold 100 KeV.
- Neutron threshold for high energy at 20 MeV.
- EMF (ElectroMagnetic FLUKA) on.
- The threshold for primary and secondary charged particles of Multiple scattering at minimum allowed energy.
- In elastic Compton profiles and Compton scattering active.
- Hadrons/muons and EM particle ionization fluctuations are restricted on.
- Tabulation ratio for hadron/muon dp/dx set at 1.03, fraction of the kinetic energy to be lost in a step set at 0.02.
- Fully analogue absorption for low-energy neutrons (below 20 MeV).

5.5.2 Source card

This card reads the Source.f routine, in Figure 18, which contains information of energies used in the TPS, patient position as well as the Gantry angle, and all spot information used in the treatment, i.e. the spot weight, sizes, and positions.
All this information has been extracted from the PBS DICOM plan by using the Sort_dicoms_impt.py script.

5.5.3 USERWEIG card

Treatment planning systems normally calculates and reports dose-to-water as this is the standard form of reporting dose in radiotherapy(Harald Paganetti, 2009). In contrast, FLUKA MC calculates dose relying on material scoring, which initially makes comparisons of dose between the two systems hard. Through the fluscw.f routine we can however achieve the scoring of dose-of-water also in FLUKA by using the USERWEIG card as Figure 17 displays, the dose-of-water have calculated by using the equation below :

$$D_w = \Phi_m \frac{LET_w}{\rho_w}$$

D_w, represent Dose-to-water.

Φ_m, charged particle influence in a given medium.

LET_w, linear energy transfer in water.

ρ_w, water density.

5.5.4 Voxel card

A detailed patient geometry is described in practice in the shape of voxels, via three-dimensional grid space. Each voxel composed of material and density information of patient geometry and it is memorized in voxel files. FLUKA is able to process voxel files using a VOXEL card, which is created from DICOM CT images using the Flair graphical user interface. In this project, the voxel file was determined after using the set_HU.py script over all DICOM CT images.

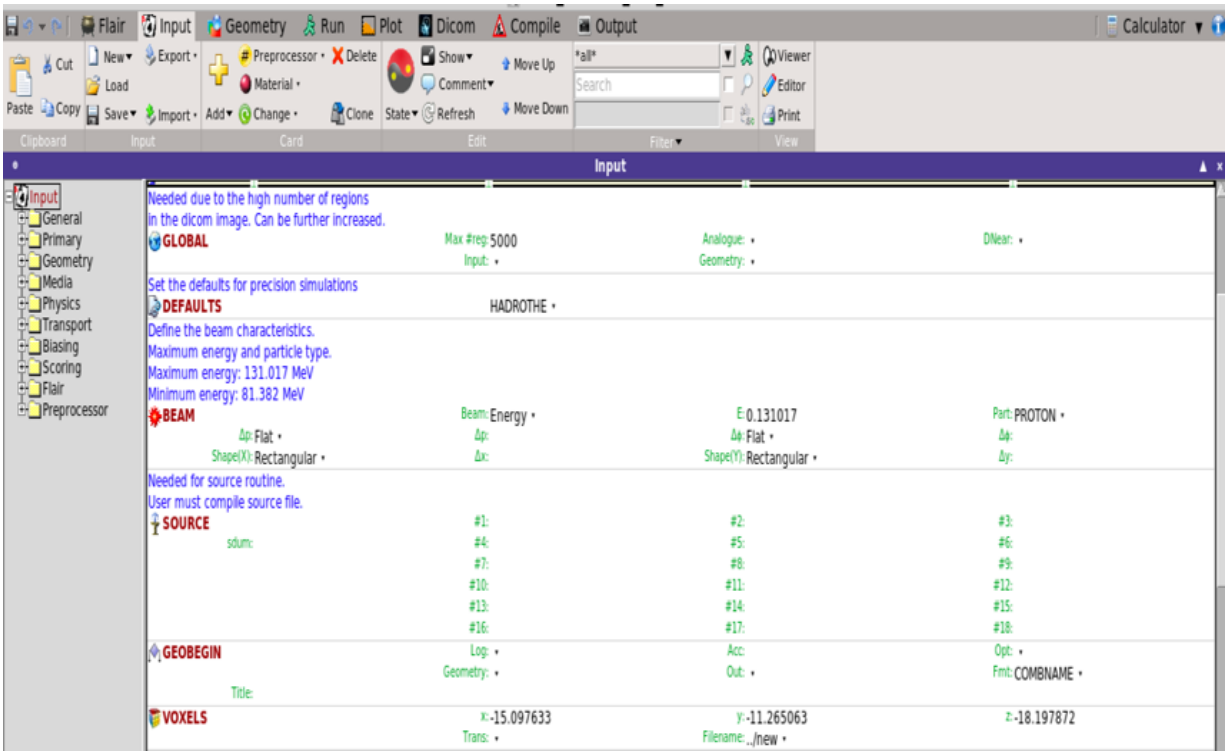

Figure 18. Illustrations of DEFULTS and SOURCE cards on FLAIR.

5.1.1 Simulation resources and data processing

5×10^6 primaries for 24 parallel simulations have been used for each treatment beam field, giving a total sum of 1.2×10^8 primary protons. The whole CPU time period to achieve 24 parallel simulations was 4 hours for a single beam field only and for to two beams filed combined it was 8 hours.

Each treatment field used 5×10^6 primaries for 24 parallel simulations, in order to execute a total of 1.2×10^8 primary protons. A total duration CPU time in order to do 24 parallel simulations was 27 hours, and for two treatment beam fields the simulation took 54 hours. Once adding all settings required as referred above and after the simulation had been done, the parallel simulations were merged together into result files in the generic FLUKA format (.bnn-files). These were then converted to ASCII format (bnn.lis files) which finally could be used and converted to DICOM files. This was done utilizing the convert_to_dicom.py script (see Figure 16). According to the user request DICOM files contain various data can be

created based on which study required to handle of list below, for this project goal the information regarding data was chosen for the first two options from the list only:

- Dose-averaged LET (LET_d)
- Biological dose (RBE = 1.1)
- Physical dose (RBE = 1.0)
- LET-weighted dose (C x LET_d x physical dose), where C must be provided by the user.
- Neutron dose
- Biological non-linear models (Rørvik weighted, Mairani, and Belli).
- Biological linear models (Wilkens, Wedenberg, Caribe, McNamara, Chen, Frese, Jones, Tilly and Rørvik unweighted).

5.8 Running LET estimation on Eclipse-Micro-Calcualtion

The water phantom and patient plan were created and analysed in the Eclipse treatment planning system as Figures 19 and 20 shows, the dose calculated with regular pencil beam convolution superposition (PCS) algorithm (Version 15.6.06) in Eclipse.
The Micro-Calculation script has been included in the algorithm, which can calculate various choices, for instance, calculate dose, LETd, Micro LETd, yD, and the RBE base on McNamara or MKM model. After running the scripts, it was utilized the options of calculating dose, LETd, and McNamara model for water phantom and patient treatment plan as seen in Figures 21 and 22. The LETd of the script is based on the unrestricted linear energy transfer calculated by conventional methods using a stopping power curve (not micro-dosimetry) and in this work it has been chosen due to the LETd calculated by MC FLUKA to the same patient plan was based on the unrestricted LETd also. Values were entered of the alpha/beta ratio for PTV and OARs is 10 Gy and 3 Gy for patient case respectively, in addition, the alpha/beta ratio for the PTV and body-water phantom is 2 Gy

used to calculate RBE by McNamara model as shown by Table 5 and in Image 23 and 24 for the water and patient case.

Table 5. Alpha/beta ratio utilized for calculated RBE-MCN for all studied cases.

Water Phantom	alpha/beta ratio	Patient Case.	alpha/beta ratio
PTV	2 Gy	PTV	10 Gy
Body	2 Gy	Brainstem	3 Gy
		Temporal lobes L	3 Gy
		Temporal lobes R	3 Gy
		Hippocampus L	3 Gy
		Hippocampus R	3 Gy

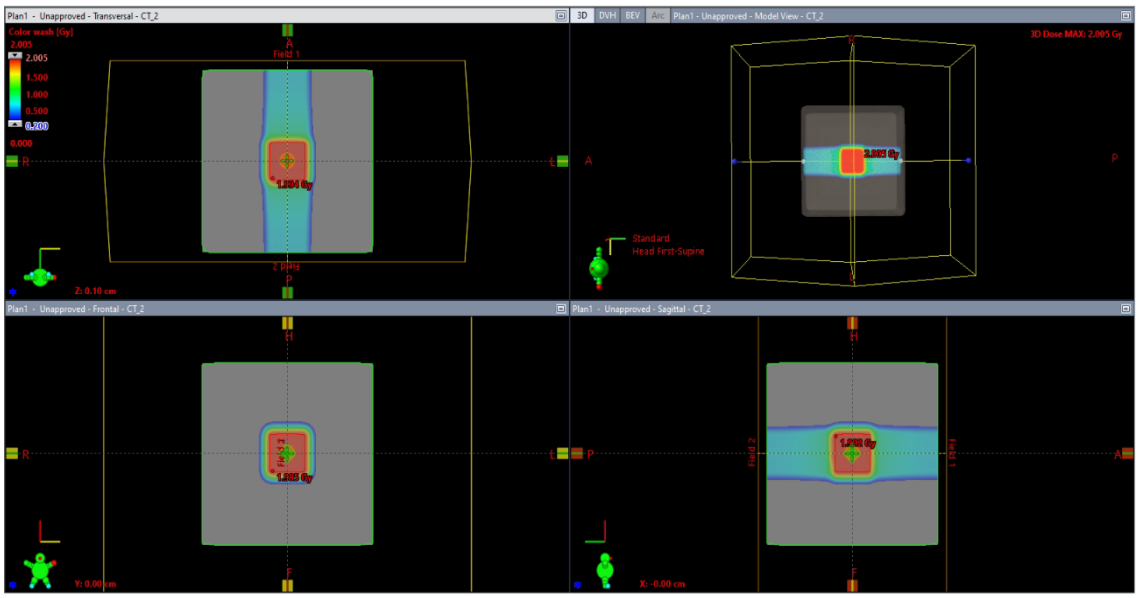

Figure 19. A water phantom on Eclipse (TPS) for Field-1 and Field-2 on PTV region represented in the red cubic shape.

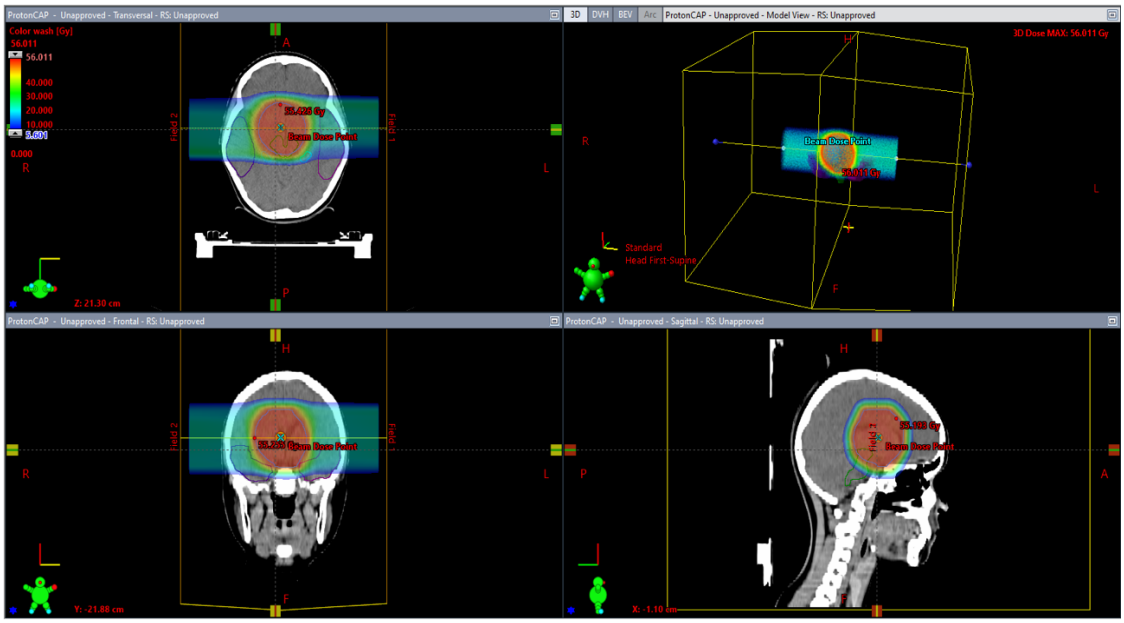

Figure 20. A Patient plan on Eclipse (TPS) for Field-1 and Field-2 on PTV region and OARs.

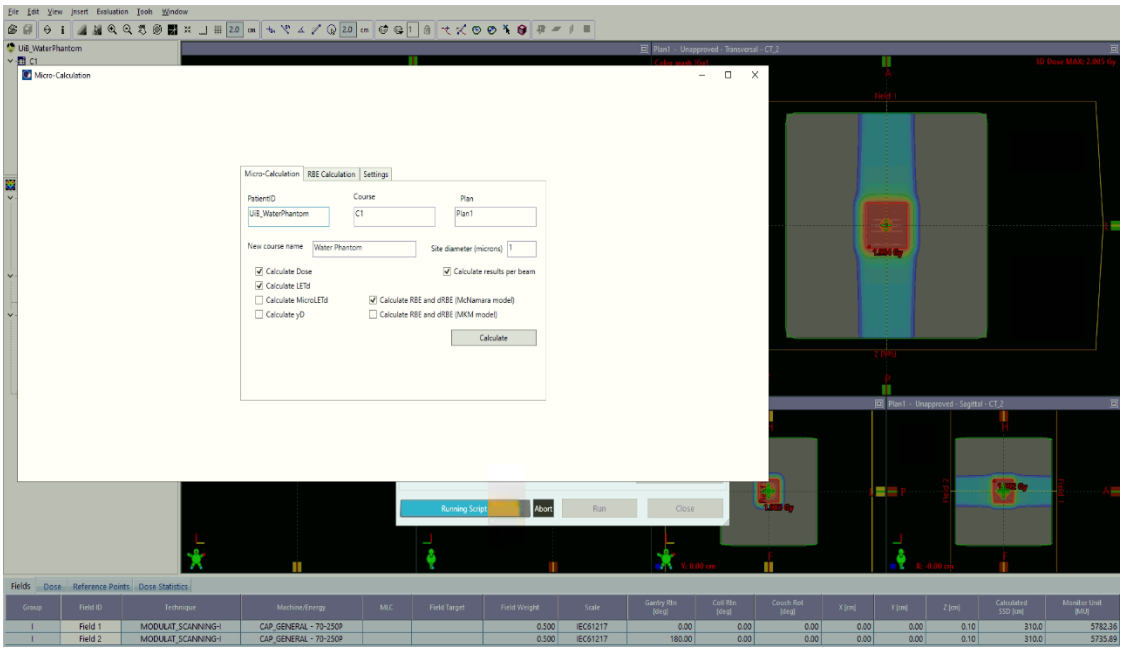

Figure 21. Options Eclipse MC-script of water phantom.

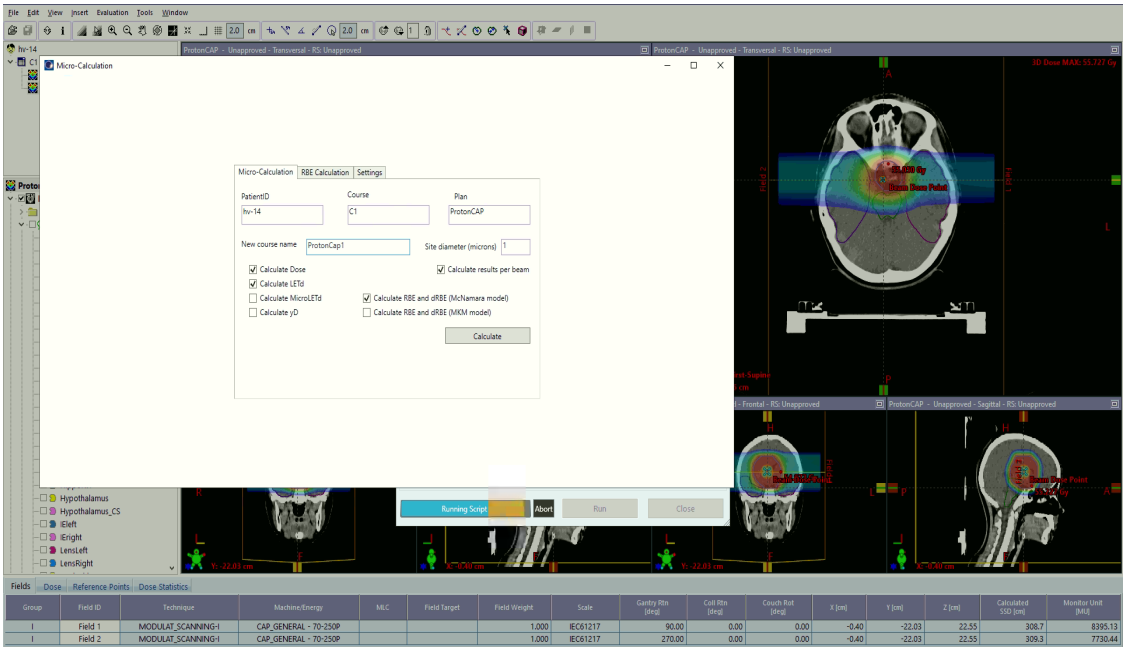

Figure 22. Options Eclipse MC-script of patient plan.

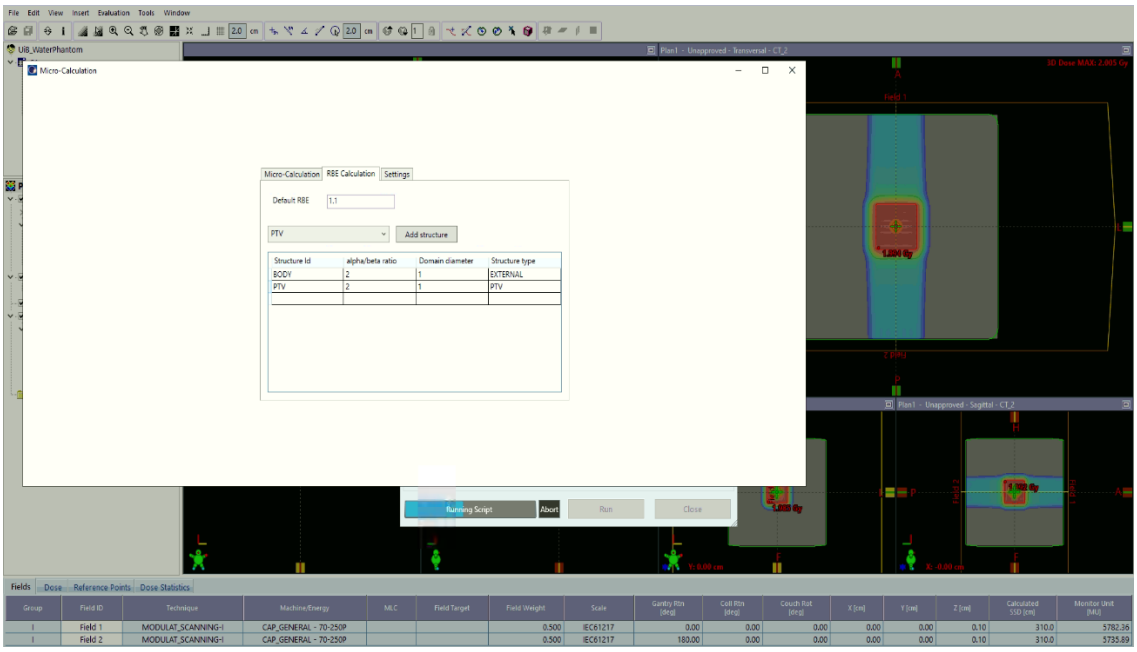

Figure 23. Assignation of Alpha/beta values of water phantom PTV.

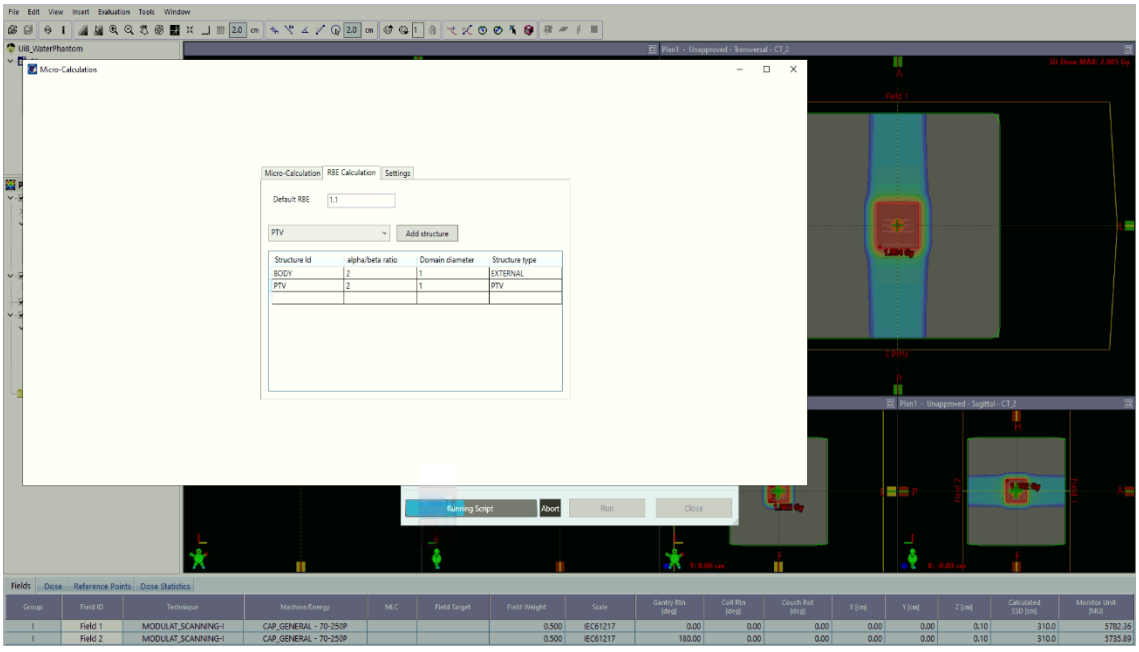

Figure 24. Assignation of Alpha/beta values of patient PTV and OARs.

5.9 Visualisation and Extraction of Metrics

5.9.1 Plot Dose-distribution

In order to compare the dose distribution from the TPS and FLUKA, visualization of the distributions was obtained by utilizing the script named plot_dicom.py. This script plots the TPS and FLUKA biological dose and dose distribution as two-dimensional(2D) color wash transported over a DICOM CT image, as well as plotting the difference of dose calculation from FLUKA and the TPS.

5.9.2 3D Slicer

The RT dose DICOM files extracted after the simulation, was used to plot Dose-volume-histograms (DVH) through using an open-software for viewing medical images and informatics called 3D-Slicer (v.4.11.0). Slicer translates the DICOM CT image and enables the user to create the DVH of DICOM files(Pinter, Lasso, Wang, Jaffray, & Fichtinger, 2012).

5.9.3 Plot Dose and LETd volume-histogram

Once the simulation had done, the data had been exported of dose and LETd data required to plot volume-histogram, VH, for all study plan, and for LETd VH, the data was extracted from Eclipse (TPS) software as DICOM format, the data of both used it in 3D Slicer to export an information used to plot a VH scheme via Microsoft Excel.

6. Results

In this section, the results obtained from both the Eclipse-treatment planning system technique and the FLUKA MC recalculation technique will be displayed. This includes the dose, LETd and RBE-weighted doses of both the water phantom and patient treatment plan. In addition, an inspection of the differences in LETd and physical dose calculated with the FLUKA recalculation and with Eclipse Micro-calculation script and finally, a comparison of the RBE values estimated from the McNamara model and the fixed RBE of 1.1 is shown.

6.1 Water Phantom results

6.1.1 Comparison of RBE 1.1. dose

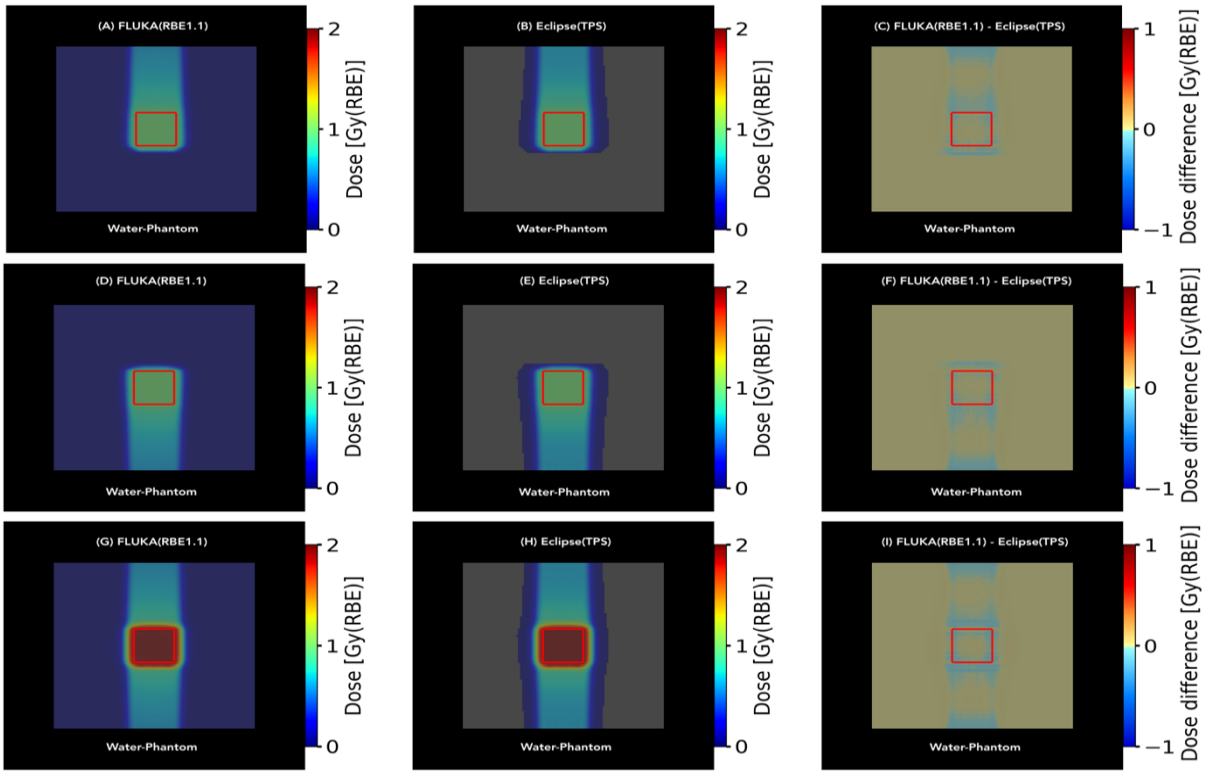

Figure 25. Illustration a calculation of dose distributions in accordance with both FLUKA(RBE1.1) and Eclipse (TPS(RBE1.1)), A and B for Field-1, D and E for Field-2, G and H for All-Fields with shows the dose difference of them on the right side, the PTV is delineated with a red cubic shaped.

Figure 25 shows the biological dose calculated with FLUKA(RBE1.1) and Eclipse (TPS(RBE1.1)) and the corresponding dose differences for the water phantom plan. The dose difference indicates small differences of dose calculate between of FLUKA and Eclipse (TPS) techniques, it can be observed that the PTV middle region in order to All-Fields status the dose through the FLUKA technique is little higher than Eclipse (TPS) technique, at the same time the outer and inner rim of PTV region, it was observed the Eclipse had a little higher than FLUKA. In Figure 26 the dose-volume histogram is shown, it displays a little difference among $V_{100\%}$ to $V_{60\%}$ about less than 0.06 Gy of dose calculation in

connection with All Fields-PTV status for both techniques emphasizes. Thus, overall good agreement was seen for the dose calculation of FLUKA and the TPS, although a slightly lower dose was observed for the TPS.

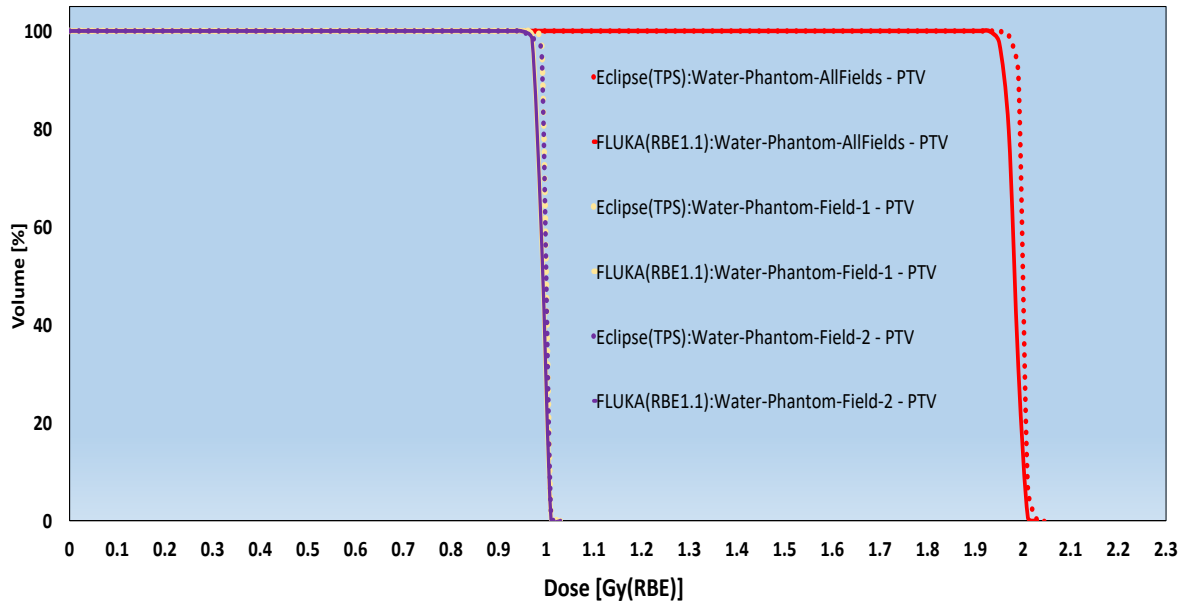

Figure 26. DVH of Eclipse (TPS), dotted-line, and FLUKA, solid-line, (both using RBE1.1) of Field-1, Field-2 and both-Fields in order to compared doses for PTV.

6.1.2 Comparison of Physical dose from FLUKA and Eclipse Micro-Calculation script

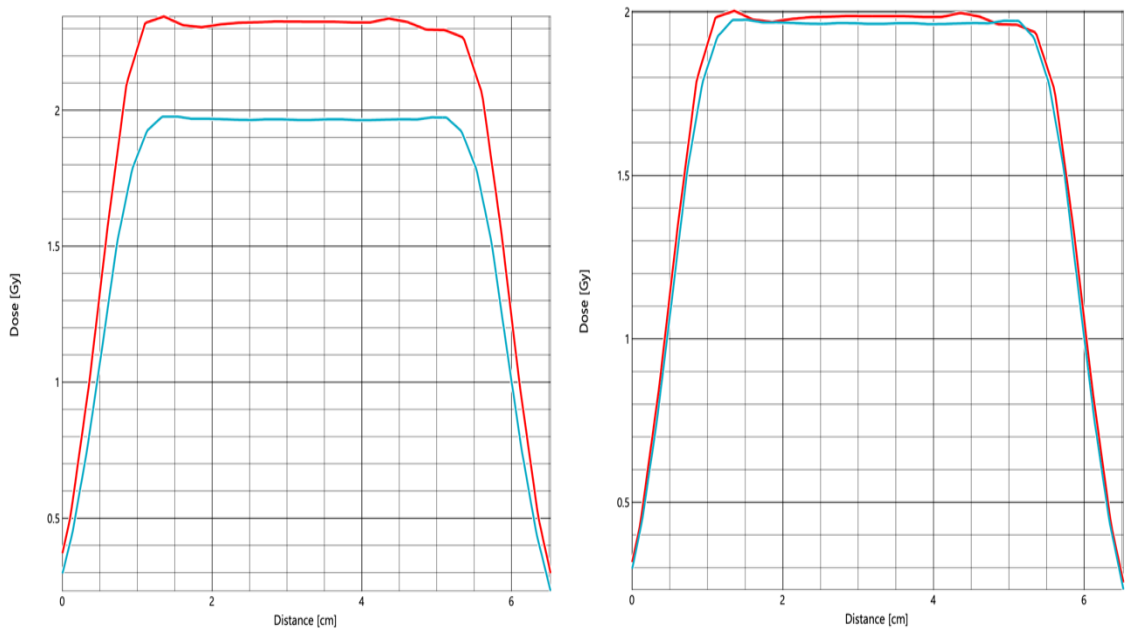

Figure 27. Dose-profile (DP) of Eclipse (TPS), light-blue line, and Eclipse Micro-Calculation, red line at PTV region, the left side represented DP before plan normalization, the right side represented DP with normalization of the Micro-Calculation plan.

The dose profile at the PTV region as in Figure 27 of the left side shows variation between Eclipse (TPS) from 2 Gy(RBE1.1), light-blue line, and Eclipse Micro-Calculation, red line, on the right side of the same Figure become with same distribution after employing 17% of re-normalization plan.

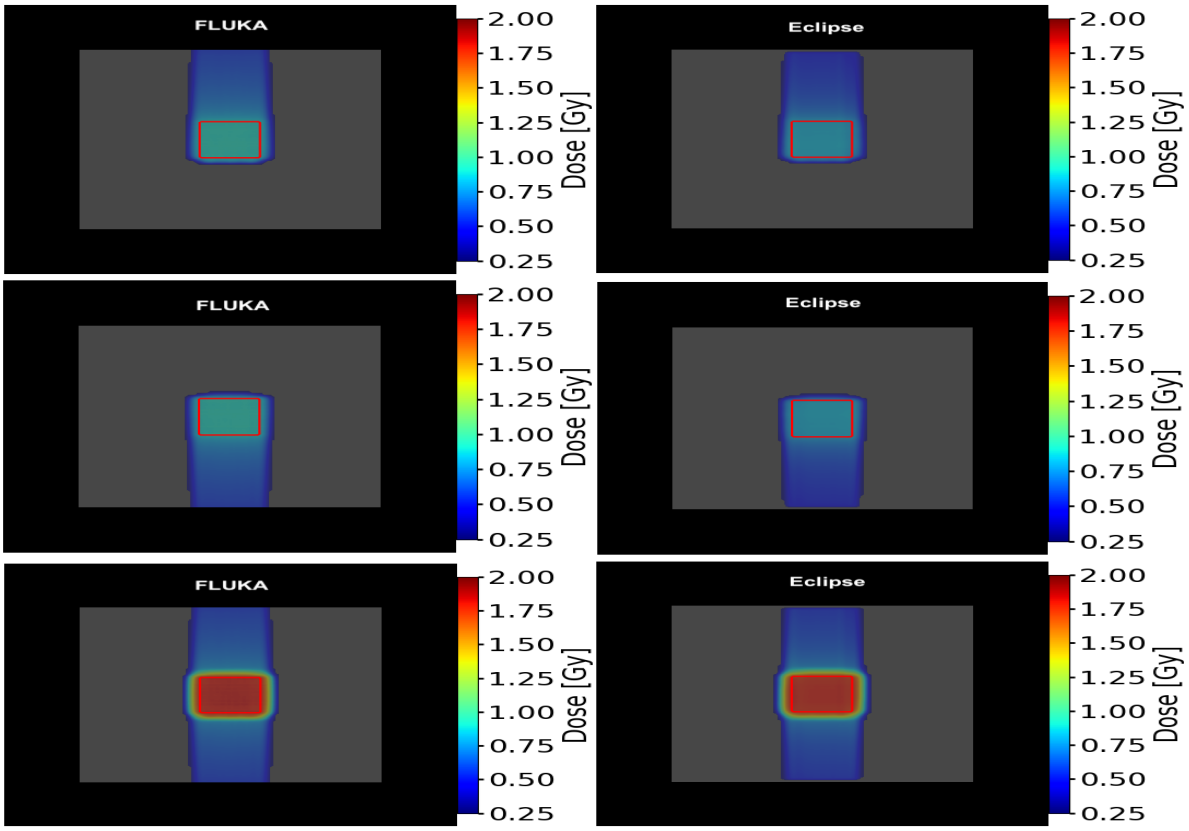

Figure 28. Illustration the physical dose of FLUKA and Eclipse Micro-Calculation script of PTV water phantom.

Figure 28 illustrates a 2D comparison of physical dose distribution of water phantom calculated through FLUKA and Eclipse Micro-Calculation script after utilizing the re-normalization plan, where the first row shows Field-1, the second row shows Field-2, and the last shows All-Fields.

It shows in Figure 28 at the status of the separate fields gave value under 1 Gy value for both methods. According to the PTV region for all fields shows convergent distribution both less than 2 Gy.

6.1.3 LET of Water Phantom

The LETd distribution and LETd volume histograms of the water phantom are shown in Figures 29 and 30, respectively, and display a disparity among the FLUKA and Eclipse LETd values. Figure 30 demonstrates Eclipse is a bit higher than FLUKA throughout all fields, the

LETd of singular field from both methods below 7 keV/μm at distal range as Figure 29 displays, likewise, for the PTV region the LETd is under 5 keV/μm for both also.

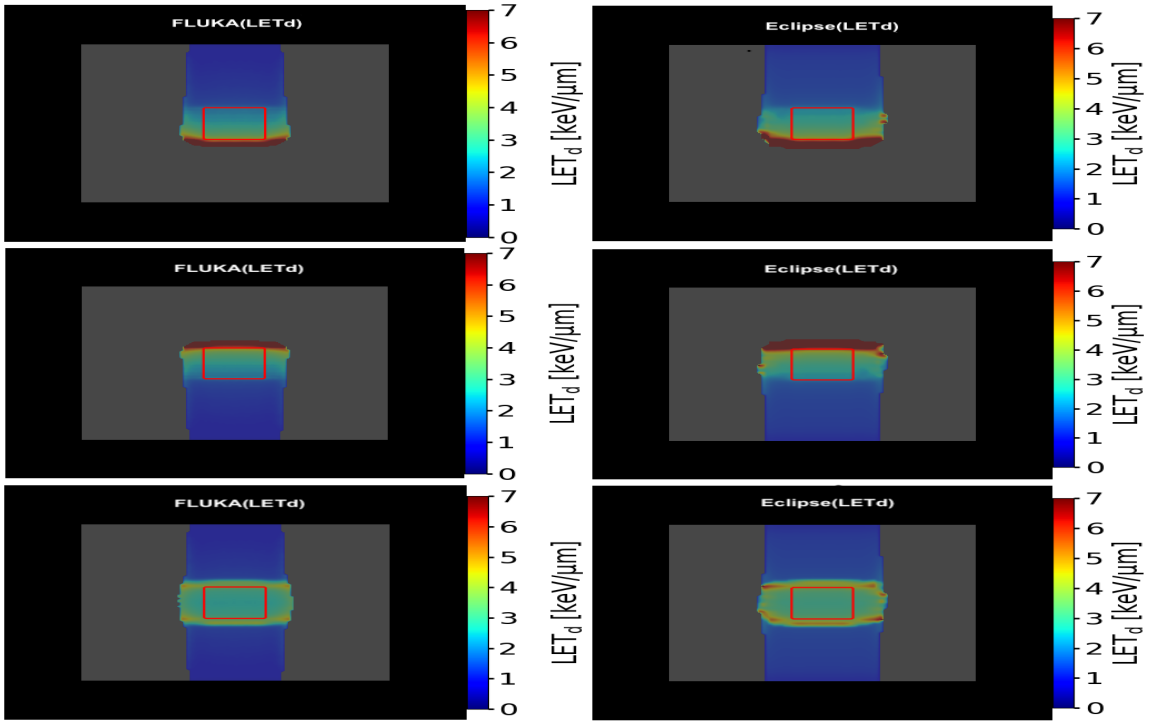

Figure 29. Illustration of LETd of Field-1, Field-2 and All-Fields row for PTV water-phantom respectively by FLUKA and Eclipse Micro-Calculation script.

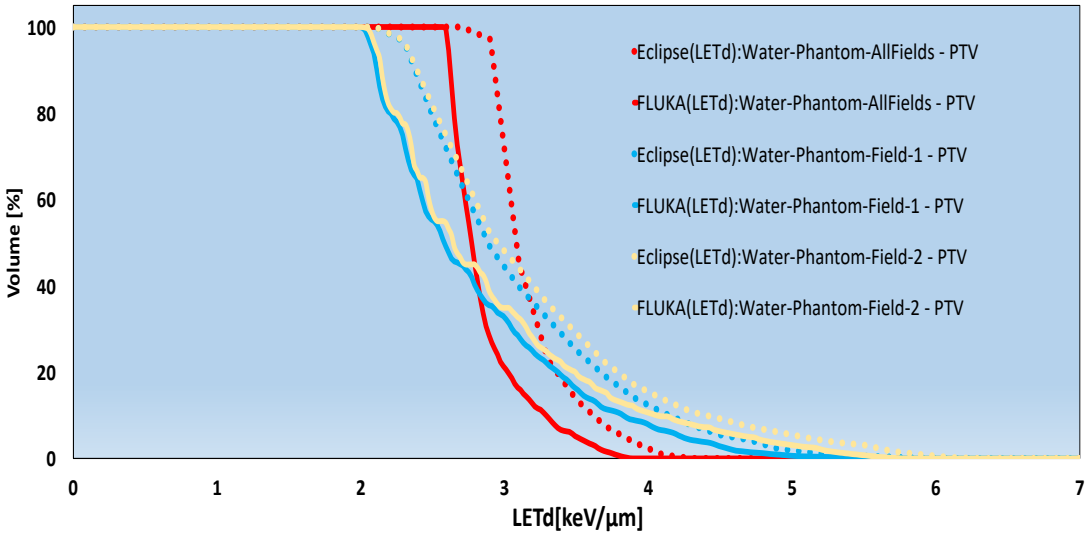

Figure 30. LETd VH of PTV water phantom by FLUKA, solid-line, and Eclipse Micro-Calculation script, dotted-line, for Field-1, Field-2 and All-Fields.

6.1.4 RBE McNamara model

In this section, the RBE calculations from FLUKA and Eclipse Micro-Calculation script are presented for the water phantom plan. The RBE was calculated using the McNamara model, the alpha-beta ratio of 2 Gy was used in FLUKA and in Eclipse Micro-Calculation as mentioned in 5.8 section.

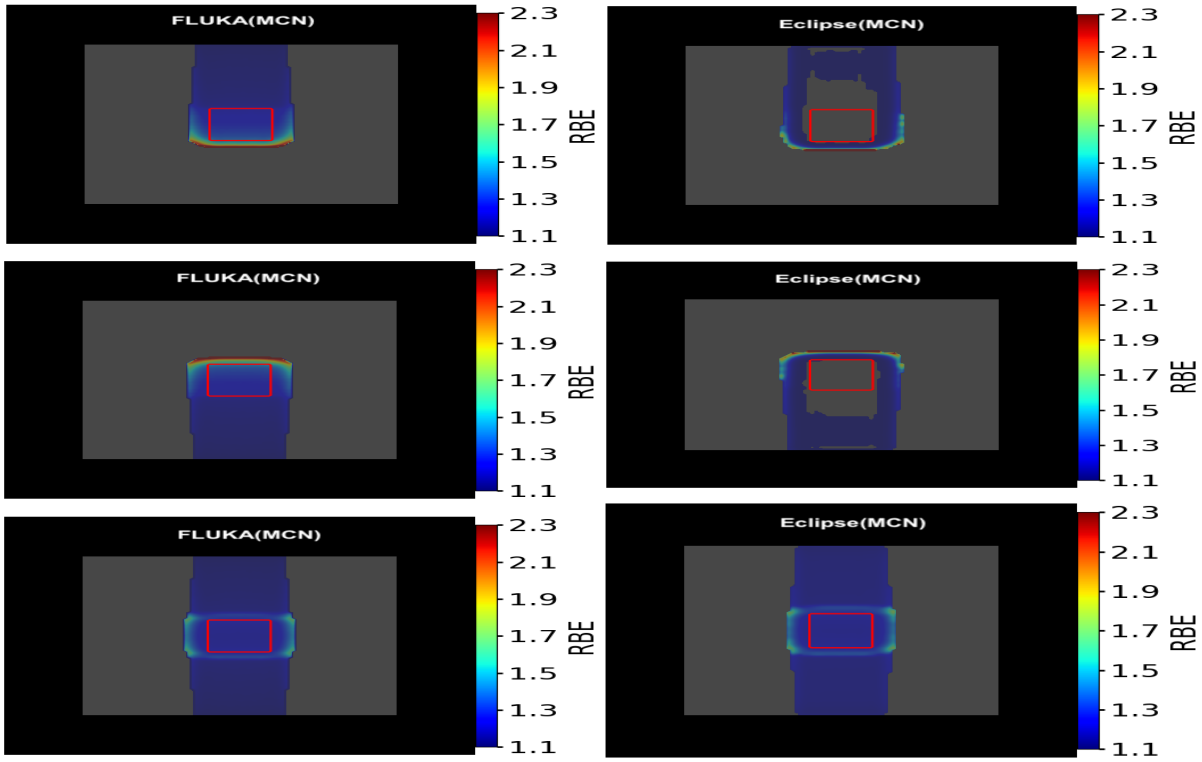

Figure 31. Illustration of RBE-MCN model for PTV water-phantom for Field-1, Field-2 and both Fields by FLUKA and Eclipse Micro-Calculation script.

The RBE values for both FLUKA and Eclipse increase towards the end of the beam, as seen in Figure 31. Field-1 and Field-2 represented by the first and second row respectively and give how differing the within the PTV region (red-cube) results of FLUKA and Eclipse calculation at RBE-MCN model. The RBE values Inside and back of the PTV were transparent for both single fields from Eclipse status which indicated the value is under 1.1 scale.

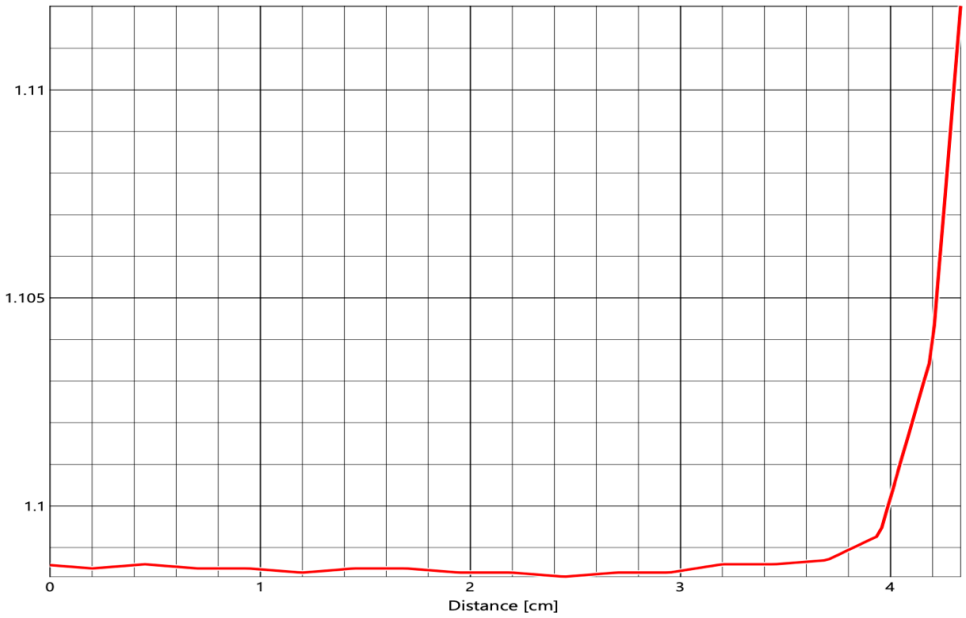

Figure 32. The RBE values within the PTV region of water phantom, Y-axis represents the RBE values and X-axis the longitudinal direction in the core Field axis of PTV region.

Figure 32 displays the RBE value within of PTV region where at the entrance of PTV, the RBE value is below 1.1 and start to increase up this value at the end of the PTV region, thereafter, the RBE value started to increase from 1.1 to reach RBE=2.3 at the front of PTV and with a low value on the side edges. About the FLUKA case, the PTV being roughly of 1.2 and it increases further at the distal edge of the field at almost reaches a value under 2.3, with constant of this value on the side edges of PTV region. Furthermore, that RBE values within PTV for both fields of Eclipse and FLUKA have ranged from 1.1 to 1.3 and take 1.7 roughly at both sides of PTV. By relating the results of both LETd and RBE, the high LETd values at distal range from Eclipse case, corresponding a high RBE value at same far range, and that what observed, and this corresponds to the positive relationship of each RBE and LETd as mentioned in 2.3.3 section.

6.2 Patient plan results

6.2.1 Comparison of RBE 1.1. dose

The dose distribution in both FLUKA(RBE1.1) and Eclipse (TPS(RBE1.1)) where RBE of 1.1 utilized in Eclipse also, of Field-1, can be studied through Figures 33, 34 and 35 which represent the dose distribution, dose-volume histogram (DVH) and Max/Mean dose respectively.

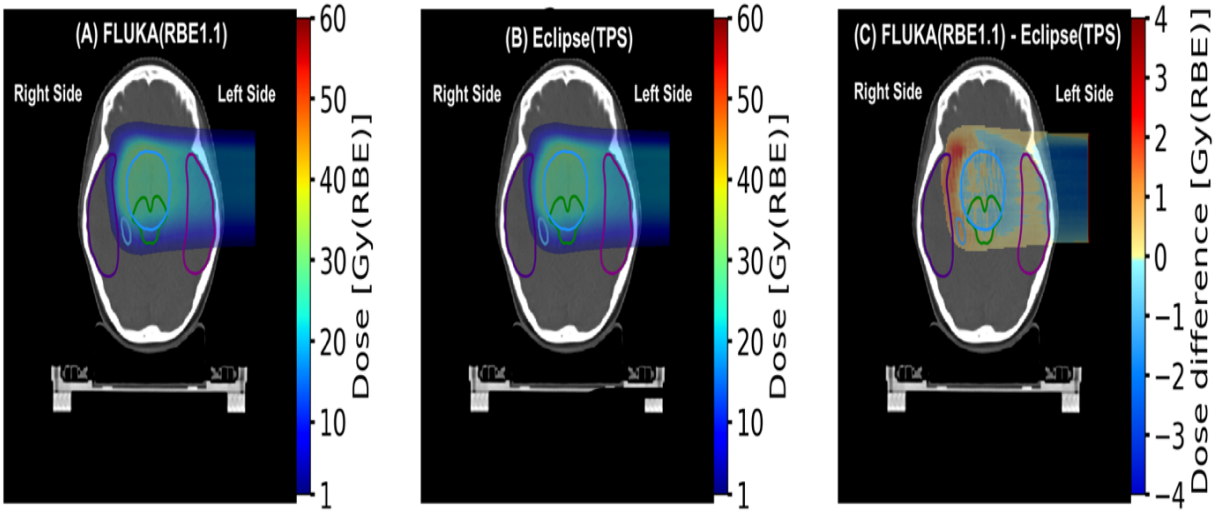

Figure 33. Illustration a calculation of dose distributions of Field-1 in accordance with both FLUKA(RBE1.1) and Eclipse (TPS) with shows the dose difference of them on the right side, the PTV is delineated with a light blue circle in addition of the OARs which includes of brainstem a green color, temporal lobes, and hippocampus for both side of head patient purple and small light blue ring color respectively.

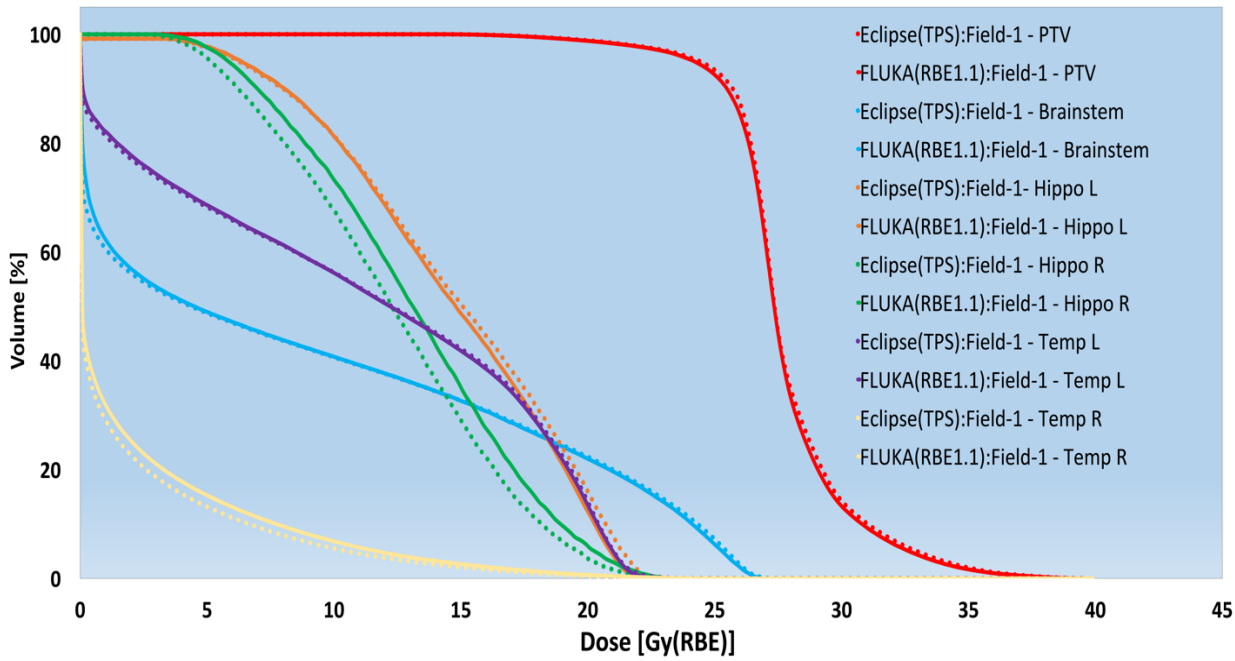

Figure 34. DVH of Eclipse (TPS (RBE1.1)), dotted-line, and FLUKA(RBE1.1), solid-line, of Field-1 in order to compared doses for PTV and OARs.

The figures demonstrate that the doses from both techniques are almost identical for the PTV region, and in the brainstem and temporal lobes-left side there is very little difference the doses. With a view to the dose temporal lobes-Right side calculated by the FLUKA(RBE1.1) technique are slightly increasing over of Eclipse (TPS) technique and apparently as shown in Figure 33-C from dose difference, the difference of dose in a hippocampus-Right appears of FLUKA(RBE1.1) technique uses, unlike the dose of in the hippocampus-Left calculated through the Eclipse (TPS) technique being close to FLUKA (RBE1.1) dose calculation value. In dose difference of Figure 33-C, the area between PTV region and temporal lobes-Right side appeared higher biological dose from FLUKA calculation than Eclipse. The scheme of maximum and mean dose displays the variation among the two techniques.

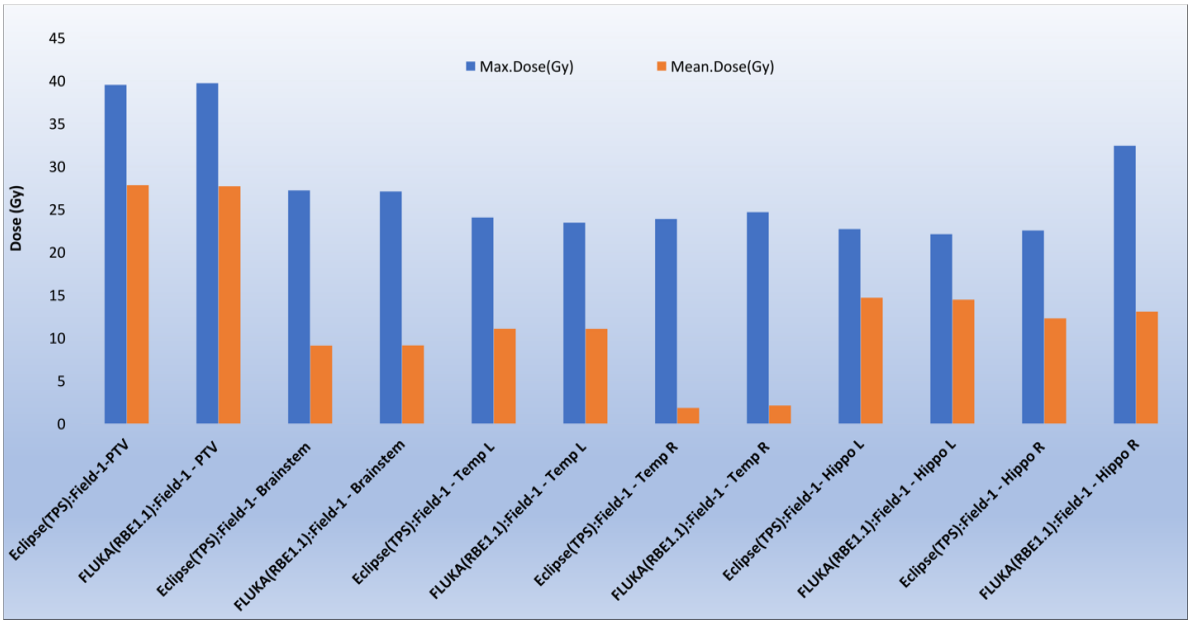

Figure 35. Scheme of maximum and mean dose for FLUKA(RBE1.1) and Eclipse (TPS) of Field-1 to the interested areas.

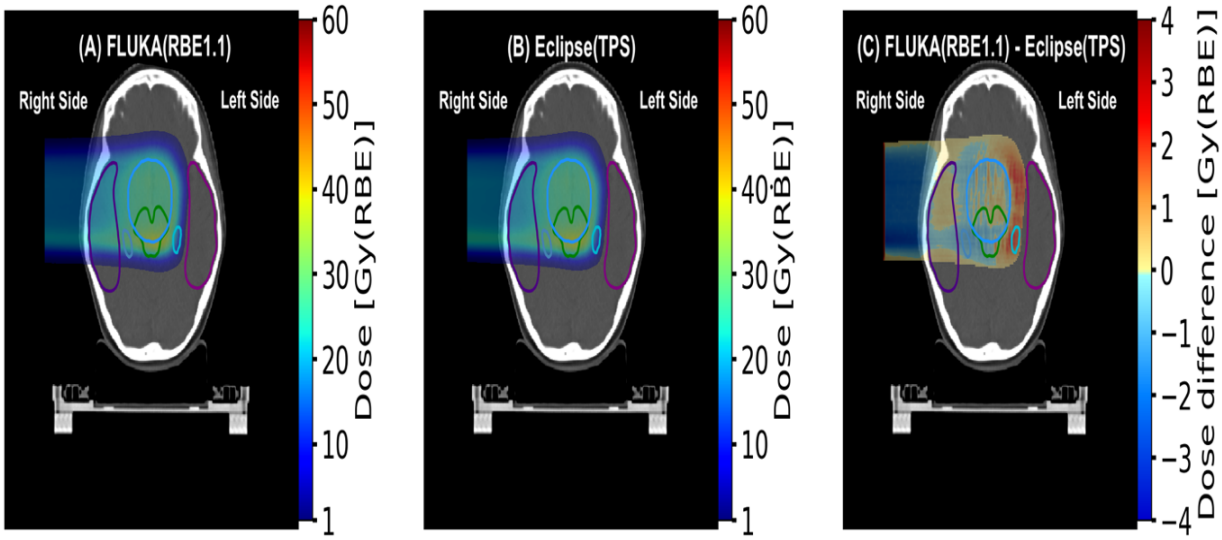

Figure 36. Illustration a calculation of dose distributions of Field-2 in accordance with both FLUKA(RBE1.1) and Eclipse (TPS) with shows the dose difference of them on the right side, the PTV is delineated with a light blue circle in addition of the OARs which includes of brainstem a green color, temporal lobes, and hippocampus for both side of head patient purple and small light blue ring color respectively.

The dose difference of Field-2 by dose distribution as Figure 36-C indicates to high dose in the area between the PTV region and temporal lobes L side for the good of FLUKA(RBE1.1) than Eclipse (TPS) and especially on the side of Hippo L, for the opposite side for the same area dose difference becomes higher for the Eclipse (TPS) this time.

Both Figure 37 of DVH and Figure 38 of Max/Mean dose for Field-2 show identical dose in the PTV region and also with a small difference for the brainstem dose and temporal lobes-Right side in both techniques, but there was an increase of hippocampus-Right side dose from the Eclipse (TPS) calculation technique compared to the FLUKA(RBE1.1) dose. There is a biological dose undesirable between PTV regional and temporal lobes-Left side the Figure 36-C showed about 3 Gy(RBE) from FLUKA(RBE1.1) and including hippocampus-Left side also . In accordance with analysing the data and figures, there is a great convergence between the two method calculations if the organ at interest not at the distal range of the field.

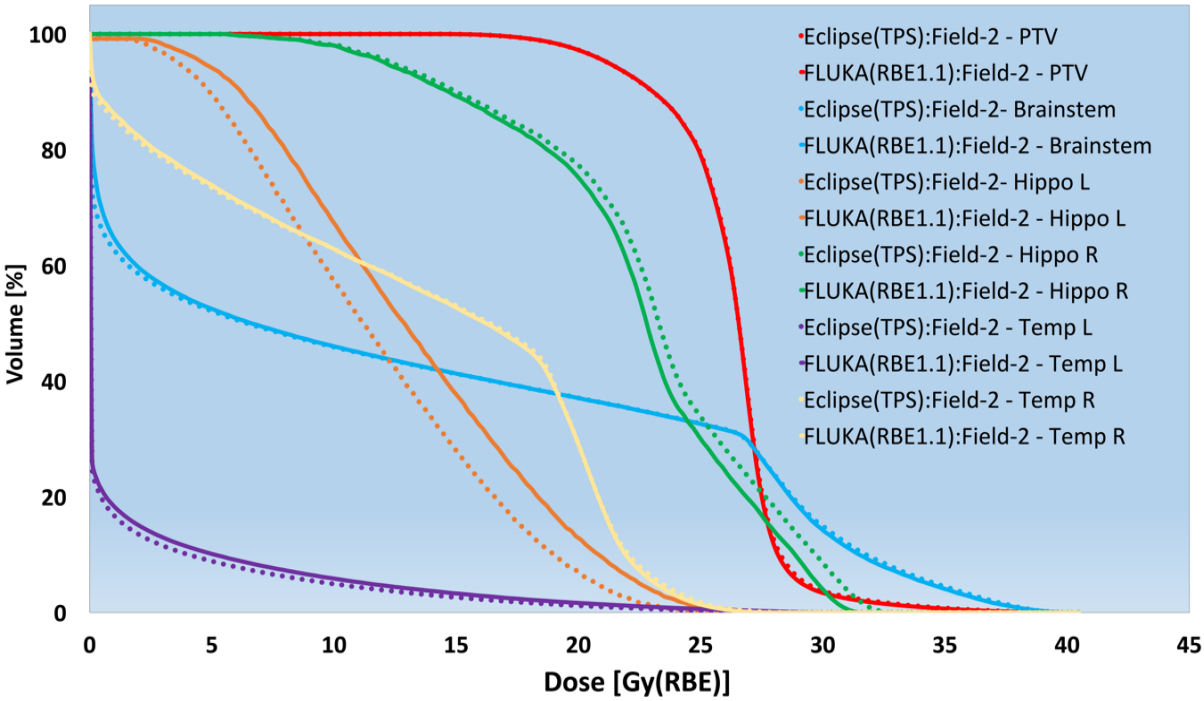

Figure 37. DVH of Eclipse (TPS(RBE1.1)), dotted line, and FLUKA(RBE1.1), solid-line, of Field-2 in order to compared doses for PTV and OARs.

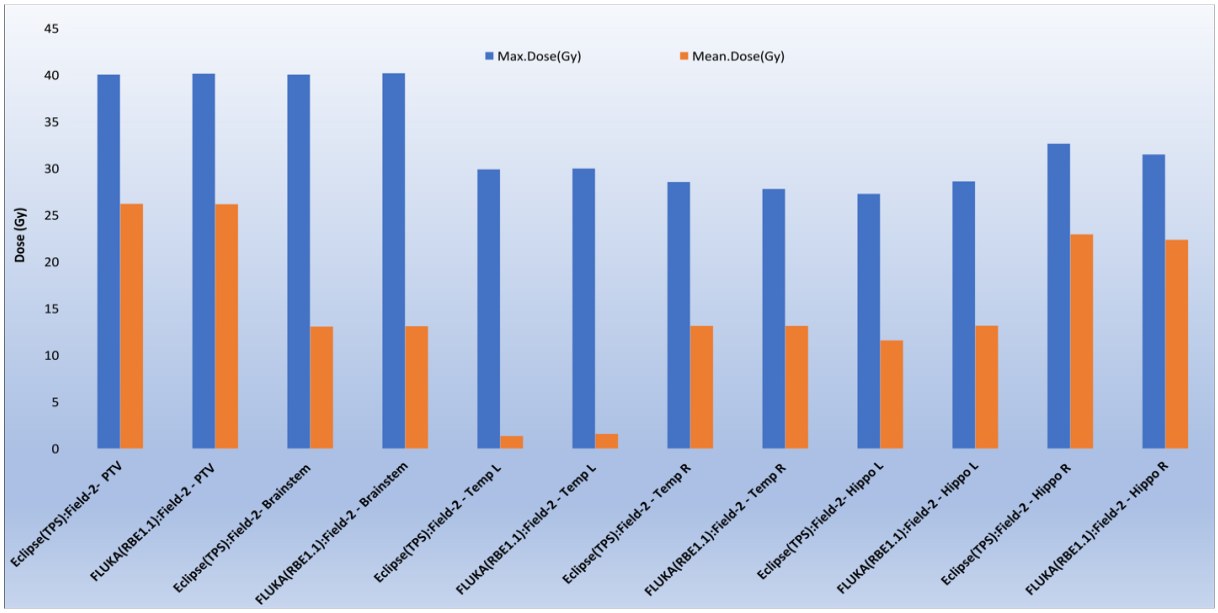

Figure 38. Scheme of maximum and mean dose for FLUKA(RBE1.1) and Eclipse TPS) of Field-2 to the interested areas.

Noticeable from Figure 39 the dose difference displays of the dose planned by both FLUKA(RBE1.1) and Eclipse (TPS). The PTV region, and both brainstem and temporal lobes of the head patient are almost completely identical with increasing a very slight difference of dose FLUKA(RBE1.1) technique calculate for the PTV region where take dose value below 55 Gy(RBE). This is confirmed by the scheme dose-volume histogram (DVH), Figure 39, where most of the OARs structures and PTV region are equal in dose except the hippocampus-Left side which shows a difference in the dose calculation of both techniques. At the same time, the hippocampus area displayed a FLUKA(RBE1.1) dose of approximately 2-3 Gy higher than the Eclipse (TPS) dose. As well as, Figure 39-C illustrates a high dose in the area between the PTV region and temporal lobes for both sides for the benefit of FLUKA calculation. Figure 41 below, illustrates the Max/Mean dose of the PTV region and the OARs, and demonstrate the close match of doses calculated using both FLUKA(RBE1.1) and Eclipse (TPS) technique. The scheme from Max/Mean dose gives a good indication of the convergence of the two calculation methods from biological dose delivery for PTV or OARs.

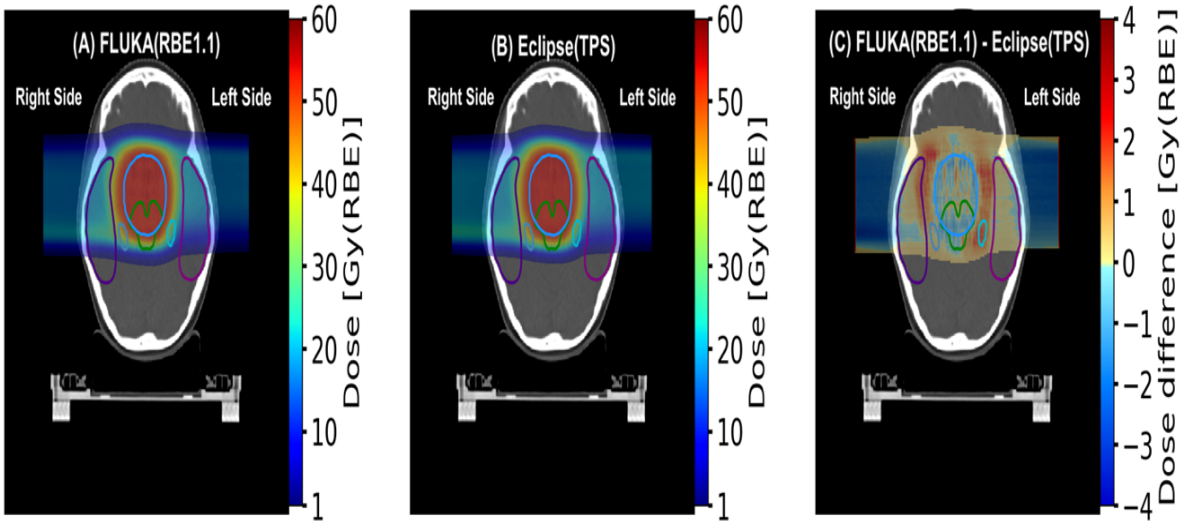

Figure 39. Illustration a calculation of dose distributions of All-Fields in accordance with both FLUKA(RBE1.1) and Eclipse (TPS) with shows the dose difference of them on the right side, the PTV is delineated with a light blue circle in addition of the OARs which includes of brainstem a green color, temporal lobes, and hippocampus for both side of head patient purple and small light blue ring color respectively.

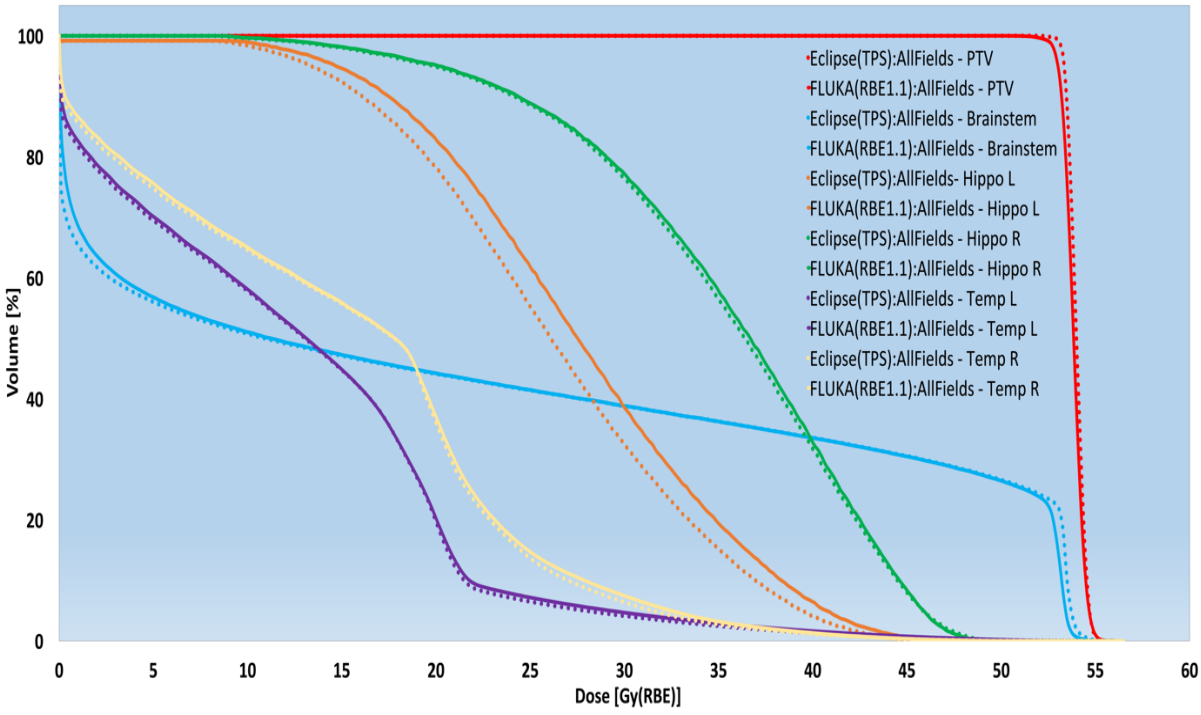

Figure 40. DVH of Eclipse (TPS(RBE1.1)), dotted-line, and FLUKA(RBE1.1), solid-line, of All-Fields compared doses for PTV and OARs.

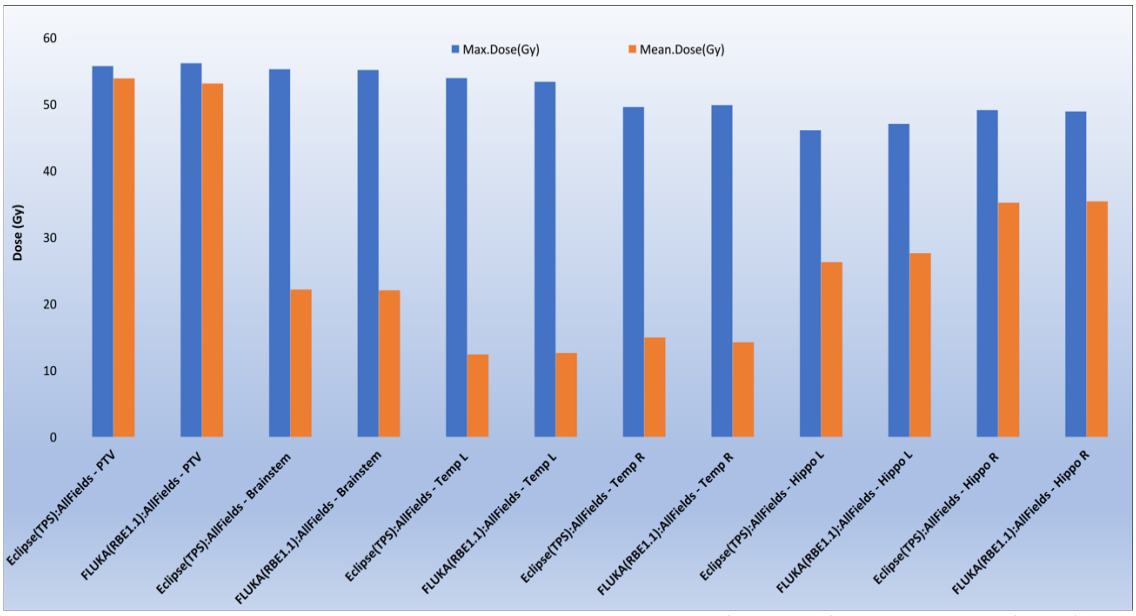

Figure 41. scheme of maximum and mean dose for FLUKA(RBE1.1) and Eclipse (TPS) of All-Fields to the interested areas.

Comparison of Physical dose calculated from FLUKA and Eclipse Micro-Calcualtion script

Through operates in the same approach of water phantom physical dose analysis, Figure 43 displays the physical dose to the FLUKA recalculation of the patient treatment plan and to the Eclipse Micro-Calculation script at 17% of normalization plan mode from Eclipse (TPS) and this shows for the right side in Figure 42, where the graph demonstrates the Eclipse Micro-Calculation biological dose pre and post normalization plan, having regard to a converging results when compared among the FLUKA(RBE1.1) and the Eclipse (TPS) biological dose distribution.

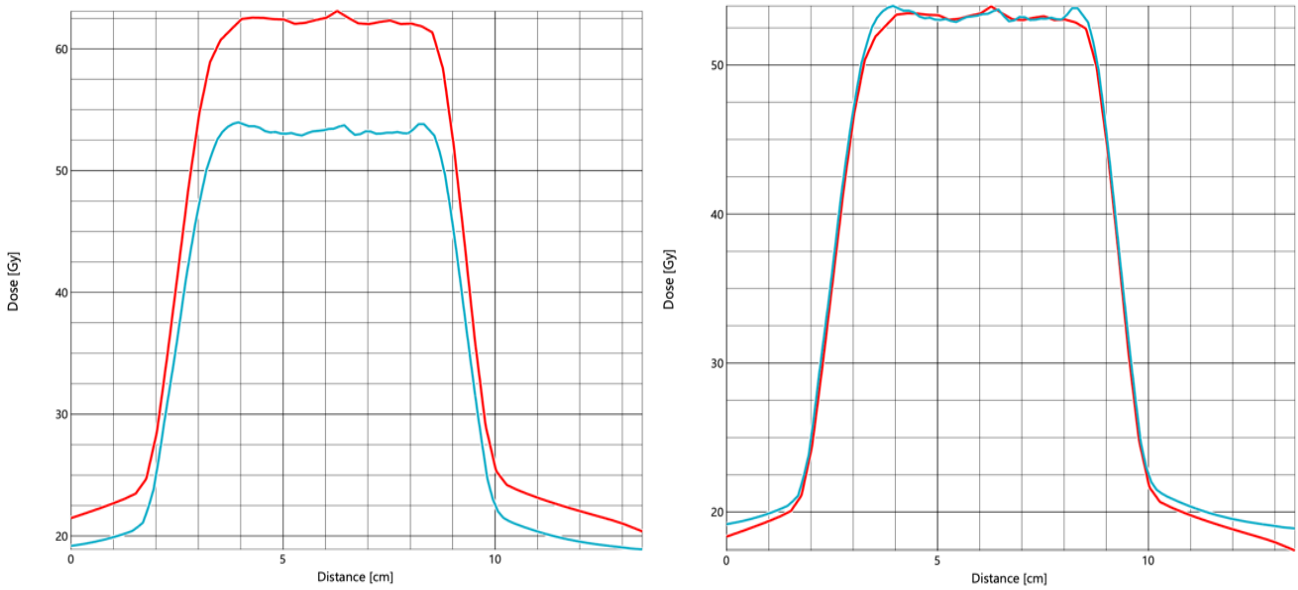

Figure 42. Dose-profile (DP) of Eclipse (TPS), light-blue line, and Eclipse Micro-Calculation, red line, the left side represented DP before normalization plan, the right side represented DP re-normalization plan.

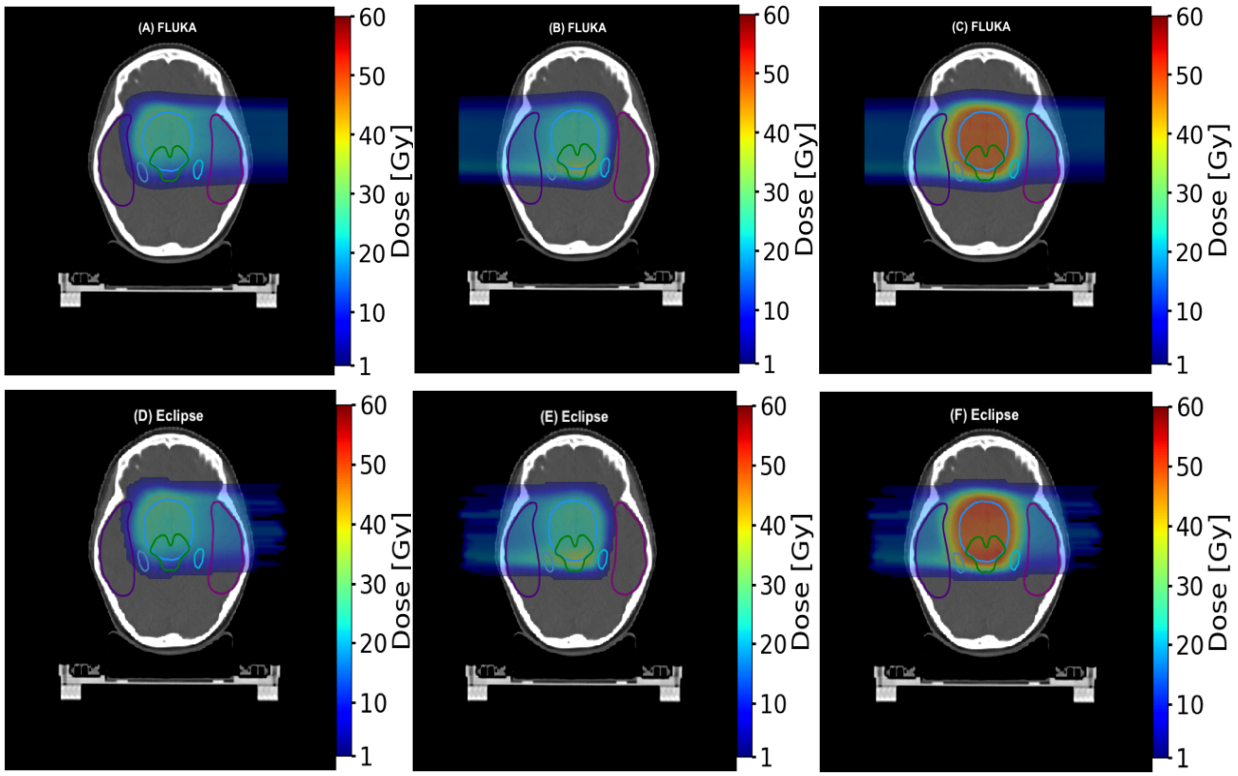

Figure 43. Physical dose distribution of FLUKA and Eclipse Micro-Calculation script for Field-1, Field-2 and All-Fields.

Through the color wash bar analysis in Figure 43, especially to the PTV position, it had been determined a PTV physical dose distribution of 49 Gy at treatment plan by Eclipse, and the FLUKA recalculation gave good and near results of the prescription dose value. However, the Eclipse Micro-Calculation script has exceeded ≈ 10Gy of dose value before normalized. Since there was a slight difference in the dose value for both methods in the case of water phantom despite the utilize of a homogeneous medium, it is expected that the dose difference will become greater when the field penetration in a non-homogeneous medium.

6.2.1 LET of Patient Plan

For the case of Field-1, through Figure 44 of LETd distribution and by Figure 45 of LETd VH, the LETd value increases as the penetration at the distal beam for both technique and it has been observed a difference in LETd computation through FLUKA and Eclipse methods, the latter shows higher LETd values compared to FLUKA on most OARs, except the temporal lobes R organ where at $V_{50\%}$ the Eclipse LETd value less than 6 keV/μm, whereas at the same volume the FLUKA LETd less than 10 keV/μm and brainstem have some different with various LETd value. By taking a peek, in Figure 44, the color wash bar of the FLUKA(LETd) and Eclipse (LETd) distribution emphasizes the outcomes at the distal range have a high LETd value corresponding with low dose distribution (see section 6.2.1).
In addition, the difference between both techniques become bigger of LETd in the organ's place located far from the beam penetration path, this appears for the place of the organs located at far of the field side, like temporal lobes R side and hippocampus R side status.
However, the PTV region different among the two methods circa/less 1 keV/μm and they have both less of 5 keV/μm value, as Figure 45 illustrates.

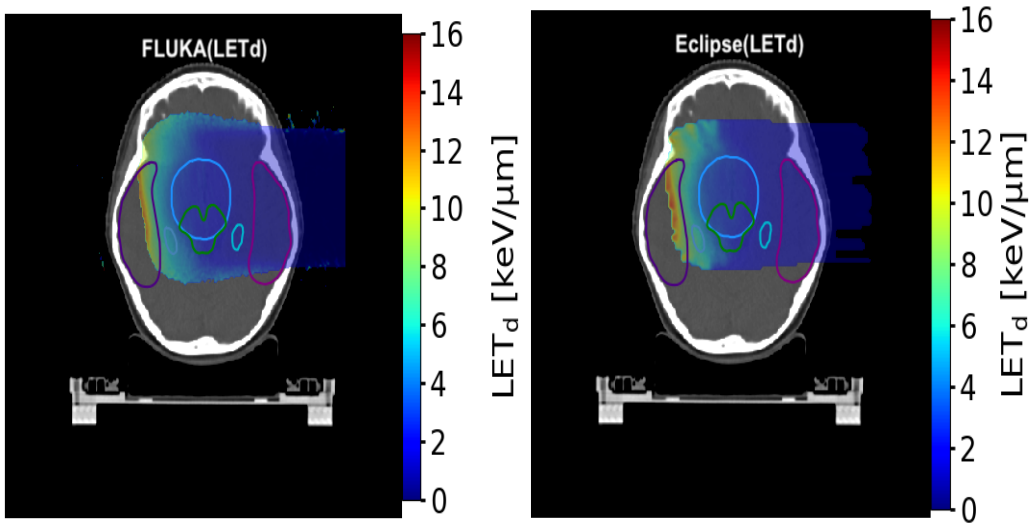

Figure 44. Illustration the LETd of Field-1 for PTV and OARs.

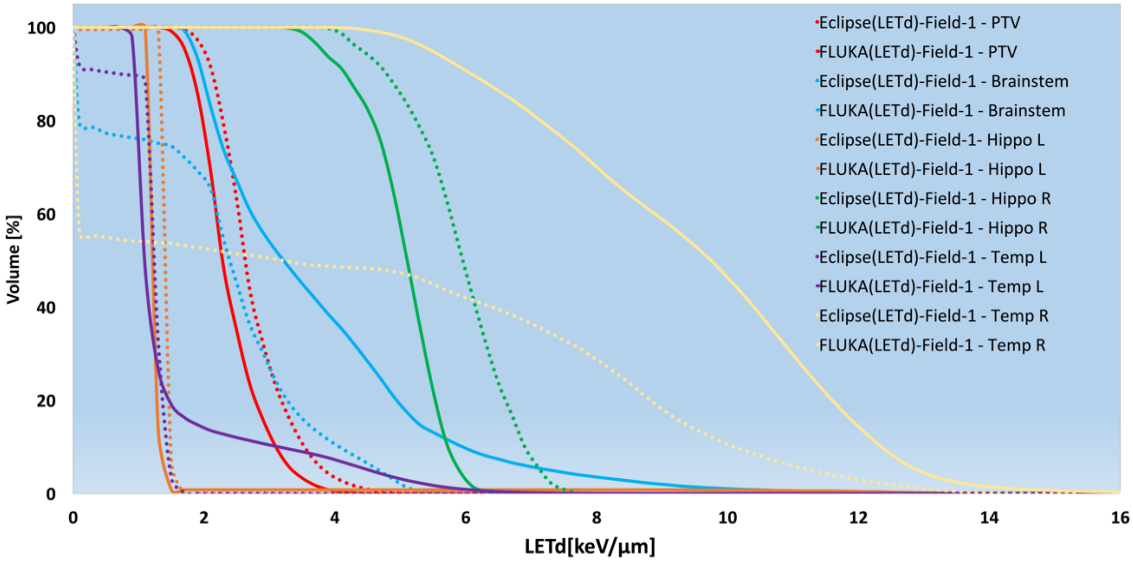

Figure 45. LETd volume histogram of Eclipse (TPS), dotted-line, and FLUKA(RBE1.1), solid-line, of Field-1 in order to compared LETd for PTV and OARs.

By inspecting Figures 46 and 47 both, we see a difference in LETd distribution and LET-VH, Figure 46 presents between the two methods with the LETd value for the good of Eclipse than FLUKA for the PTV region and some of the OARs, except the temporal lobes L side and Brainstem, tend high to the good of FLUKA. The left side organs this time have a

high difference especially for temporal lobes L side organ, at $V_{30\%}$ the LETd value takes less than 4 keV/μm value approximately for Eclipse, in contrast, LETd takes less than 13 keV/μm value for FLUKA technique. The PTV region had a similar shift of LETd value for Field-1 case.

FLUKA and Eclipse calculation with outcomes similar to the Filed-1 case again with increases LETd value at distal range of fields as Figure 46 shows, specifically for the organs located at a far distance of beams.

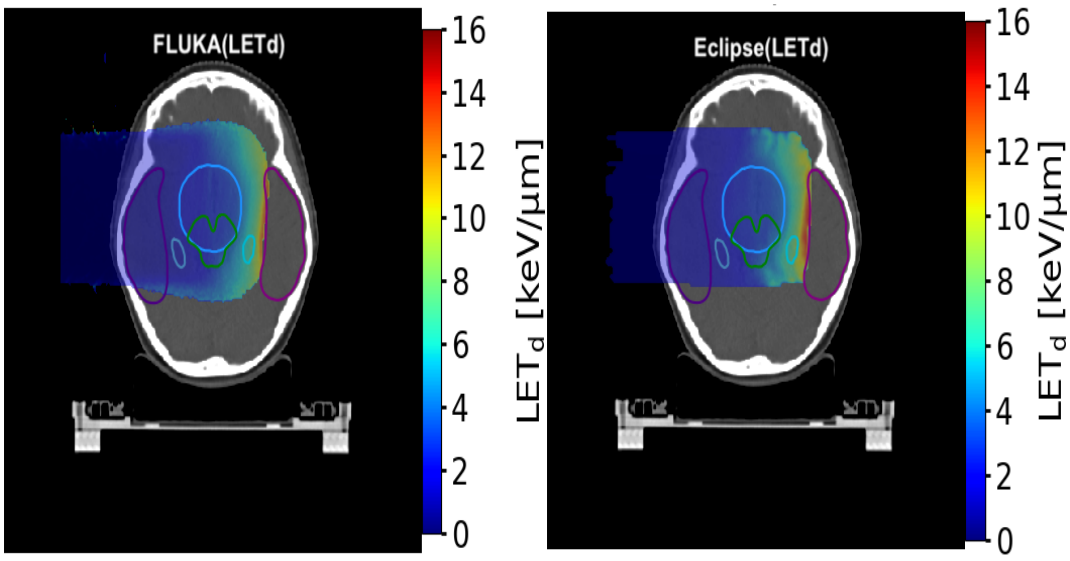

Figure 46. Illustration the LETd distribution of Field-2 for PTV and OARs.

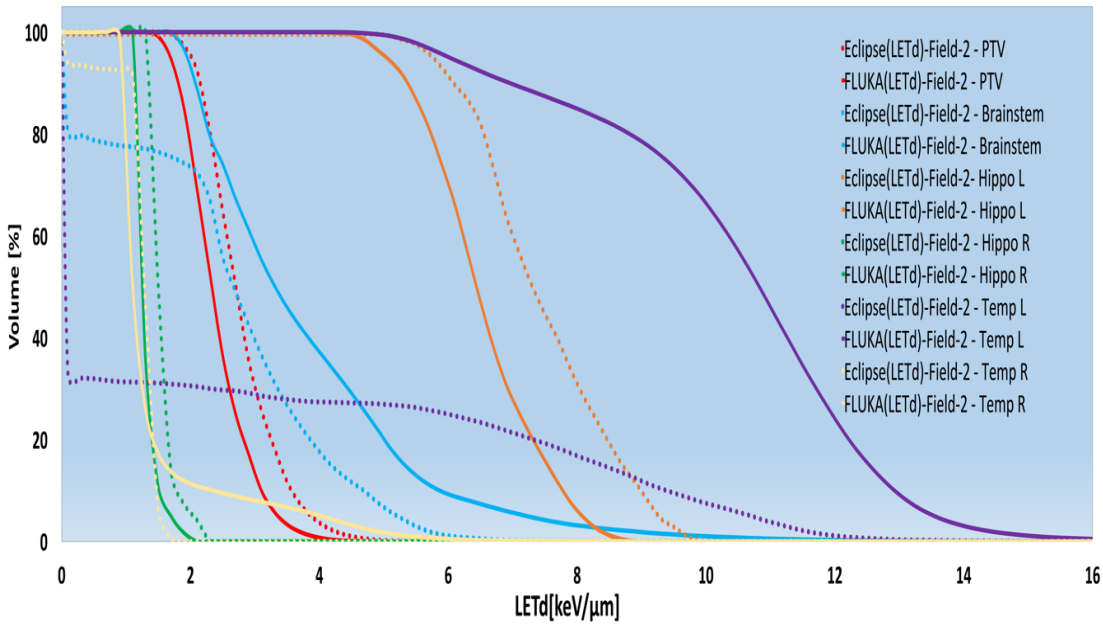

Figure 47. LETd VH of Eclipse (TPS), dotted-line, and FLUKA(RBE1.1), solid-line, of Field-2 in order to compared doses for PTV and OAR.

It found the effect of the two fields combined made LETd values of Eclipse and FLUKA less than LETd of the singular fields status with keep of LETd by Eclipse technique higher than FLUKA, and maintain LETd value of Brainstem organ at the same value roughly, as Figure 49 from LETd VH.

From the LETd VH, as seen in Figure 49, it is seen that the dissimilarity of PTV LETd values calculated by FLUKA and Eclipse preserved ≈ 1 keV/µm with reduces in a total LETd value from the case of the single fields, LETd becomes 3 keV/µm and under 4 keV/µm for FLUKA and Eclipse at attending sequence. The LETd distribution through color wash in Figure 48 shows the variation of LETd for the PTV region and OARs from both techniques in general and with eye up of on the areas upper of the PTV region of both technique in Figure 48, it found were also exposed to high LETd value, where FLUKA gave higher outcomes compared to Eclipse.

According to the biological/ or physical dose distribution from FLUKA and Eclipse, they found at each low dose region corresponding to a high LETd value as visualize by Figures 46 and 44, and the opposite is true.

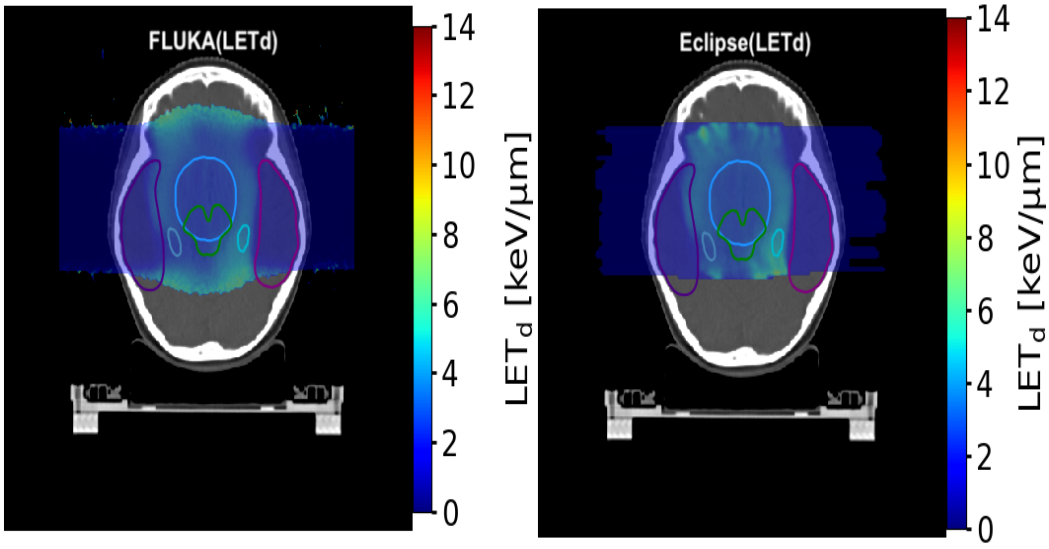

Figure 48. Illustration the LETd of All-Fields for PTV and OARs.

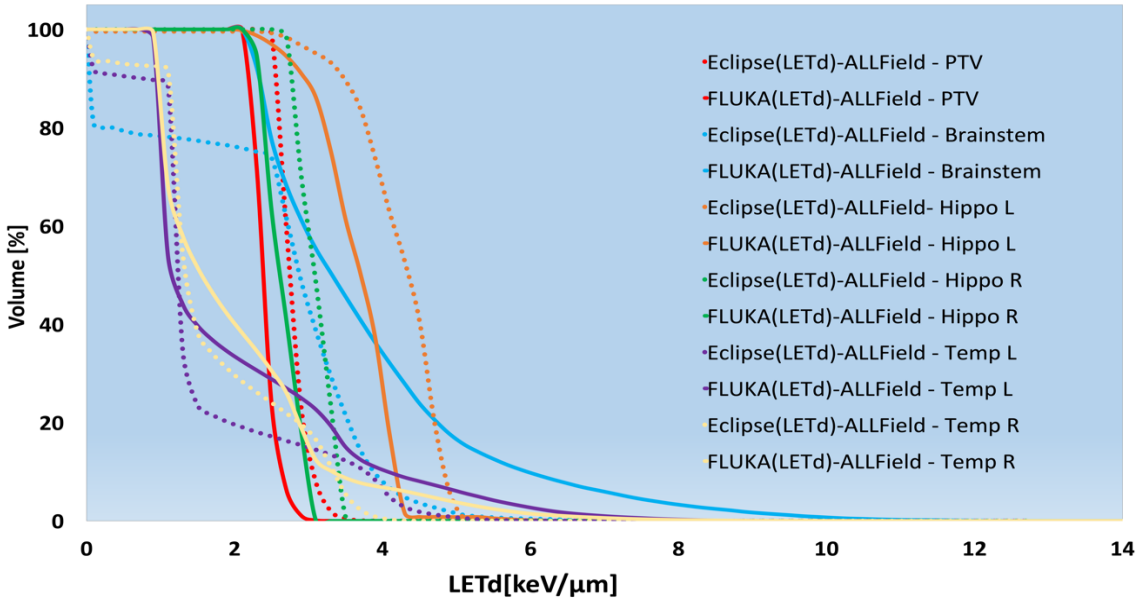

Figure 49. LETd VH of Eclipse (TPS), dotted-line, and FLUKA(RBE1.1), solid-line, of All-Fields compared doses for PTV and OARs.

6.2.2 RBE McNamara model

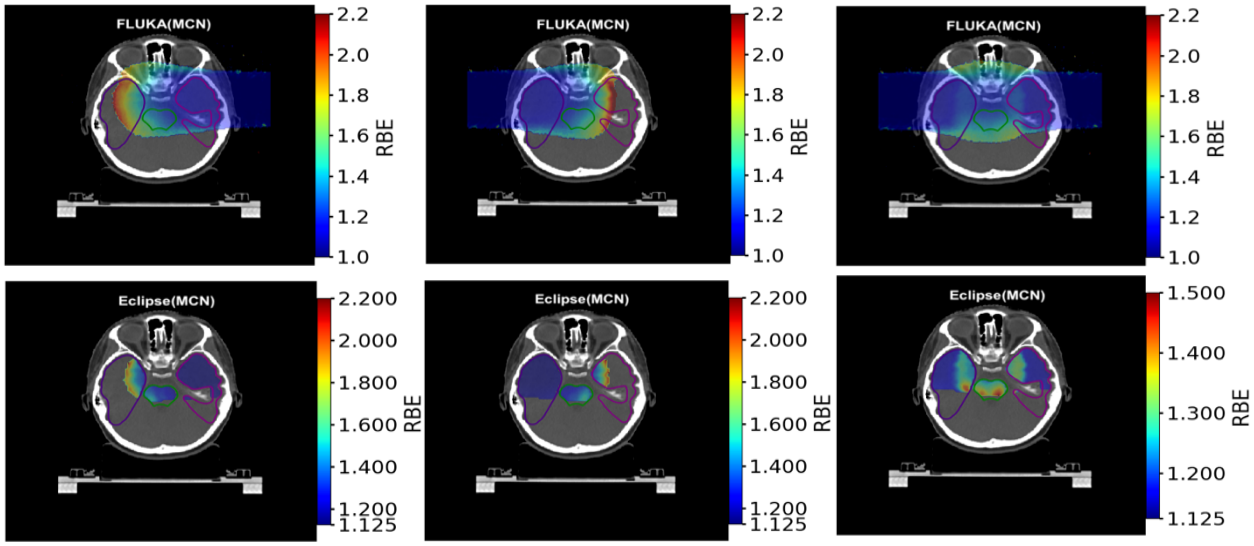

Figure 50. RBE of MCN model by FLUKA and Eclipse Micro-Calculation script for patient treatment plan, first, middle and last column represents the Field-1, Filed-2, and All Fields respectively, the first and second row presents from FLUKA and Eclipse, slice N.50.

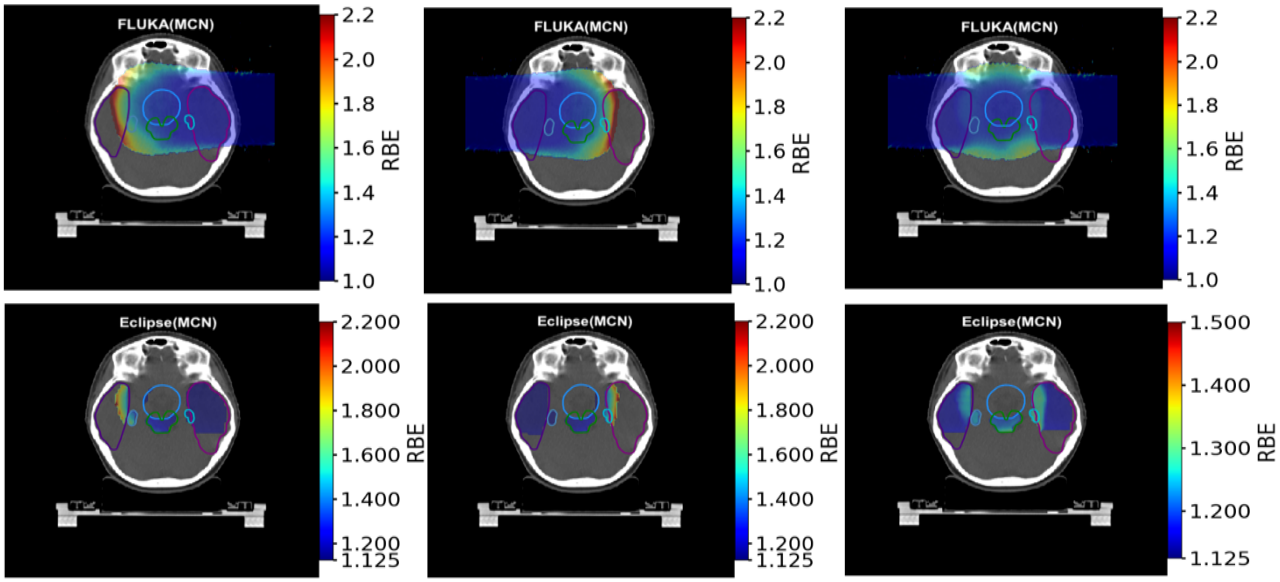

Figure 51. RBE of MCN model by FLUKA and Eclipse Micro-Calculation script for patient treatment plan, first, middle and last column represents the Field-1, Filed-2, and All Fields respectively, the first and second row presents from FLUKA and Eclipse, slice N.53.

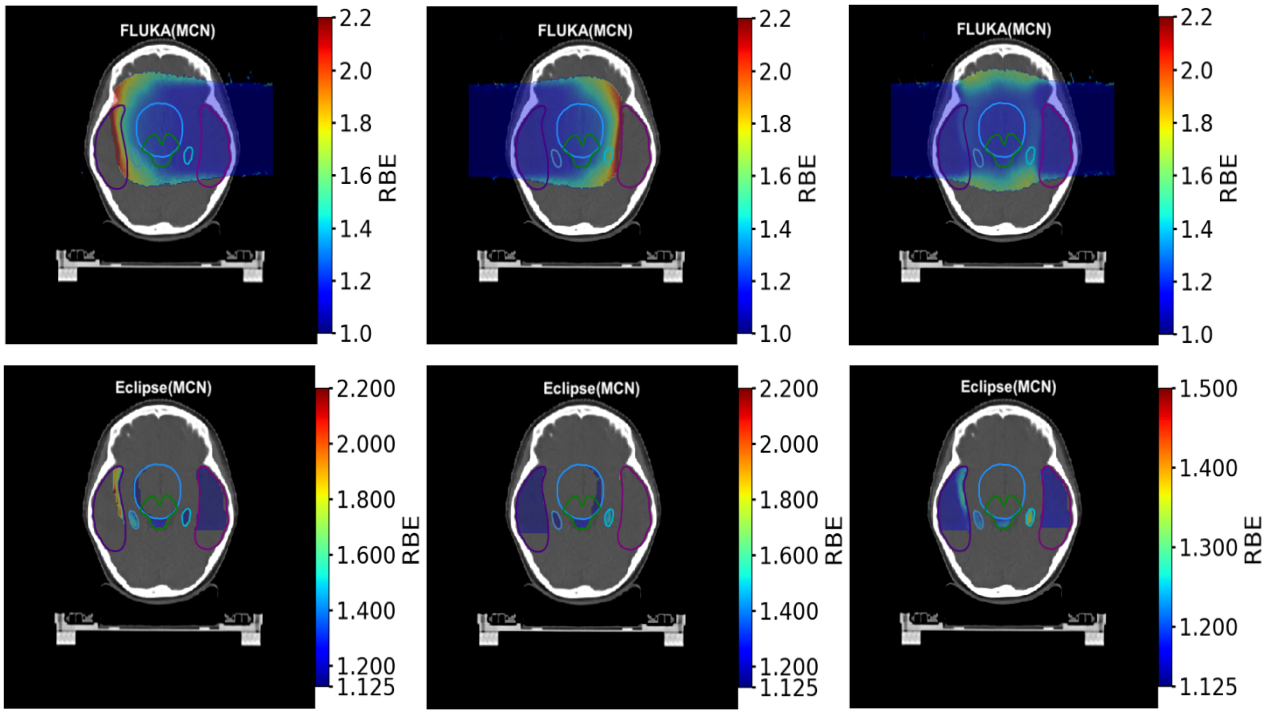

Figure 52. RBE of MCN model by FLUKA and Eclipse Micro-Calculation script for patient treatment plan, first, middle and last column represents the Field-1, Filed-2, and All Fields respectively, the first and second row presents from FLUKA and Eclipse, slice N.55.

It has been plotted different slices for each of Eclipse Micro-Calculation and FLUKA in order to attempt to show the highest RBE-MCN value for organs at interest in this study work and the extent to which the RBE-MCN correlate with the LETd outcomes generally, where the alpha/beta utilized in Eclipse as aforementioned in 5.8 section and in FLUKA 3 Gy.

Regarding to the Field-1 status, the beam inlet at temporal lobes L side region had RBE value at under 1.3 to FLUKA and at 1.125 for Eclipse with increasing of RBE value whenever the Field penetrates forward, and this show by Figure 50, the Figure 51 and 52 demonstrates RBE value of temporal lobes R side organ which take high value at 2.2 for FLUKA case and about less 2.1 to Eclipse, this RBE value occupied most of the organ's volume from FLUKA and less half organ's volume for Eclipse and this corresponded through LETd VH in Figure 45. Overall, the RBE value of FLUKA high than Eclipse status for organs in case Field-1.

Regarding the Field-2, and through temporal lobes R side this time, the RBE value take below 1.3 for FLUKA, and RBE starting at 1.125 to the Eclipse, look in Figure 50 and 51, in

addition, the RBE of temporal lobes L side takes the highest value by FLUKA of 2.2 and less this value for Eclipse, this is well shown in Figure 50 especially, the FLUKA has on a top value of RBE than Eclipse at the studied organs as in the Field-1 case also.

And back to both fields, Figure 50 demonstrates the RBE from Eclipse of the Brainstem organ has close value to the RBE from FLUKA with taking into consideration the high value for FLUKA always, the hippocampus L of FLUKA takes around 1.4 of RBE with slightly more value for Eclipse, the inner sides of the temporal lobes L and temporal lobes R have high RBE up to approx. 1.5 regarding to the Eclipse Micro-Calculation and it increases for FLUKA status.

By analysing the shapes of FLUKA for both fields, Figure 50,51, and 52, it notes areas up and down between the temporal lobes L and temporal lobes R have been exposed to high RBE reaching roughly up to 1.7.

7 Discussion

Proceeding from the water phantom status the biological dose distribution calculated by the Eclipse (TPS(RBE1.1)) method gave consequence exceed the dose prescription dose 2 Gy in the PTV region, the maximum dose, Dmax, above 2 Gy, as Figure 25-I and scheme of DVH in Figure 26 shows. The water LETd results demonstrated a small constant difference at all the volume of the PTV region either for singular or both fields from FLUKA and Eclipse Micro-Calculation, the latter had high LETd at all Fields cases, but LETd did not exceed 5 keV/μm for the PTV region, but was over this value for distal end of singular field from both methods. The RBE-MCN water phantom result concurred with LETd outcome as a linear RBE-LETd relationships for both fields of Eclipse Micro-Calculation and FLUKA, where the RBE-MCN of PTV region according to the Eclipse Micro-Calculation result came under 1.1 at singular fields as Figure 31 and 32 shows and above of 1.1 for FLUKA calculation although the Eclipse had upper of LETd valued than FLUKA, at the remote end of Field-1 and Field-2, the RBE-MCN value increased atop 1.1 as LETd raised for both methods.

Regard to the patient's condition shows great conformity of biological dose from both techniques. The outcomes indicated a suitable match in calculating the dose with the exception of some areas where there was some difference in the biological dose calculated for both methods on hippocampus L and hippocampus R side for Field-1and Field-2 status respectively as mentioned in the results chapter. In the case of singular fields, it was found that the dose in the PTV region is an almost match by FLUKA(RBE1.1) and Eclipse (TPS(RBE1.1)) and the PTV region attained the dose for both methods under 40 Gy(RBE) as Figures 34 and 37 displayed. The OARs received doses from Field -1 and Field-2 less than 30 Gy(RBE), except the Brainstem and hippocampus R side exposed 40 Gy(RBE) and below 35 Gy(RBE) respectively.

Upon returning to the sum of the total effect of the two fields together, ALL-Field state, the PTV region attained a slightly more prescription dose ≈ 55 Gy(RBE) and also Brainstem gained 54 Gy(RBE) approximately due to a near Brainstem location from the PTV region and the rest of OARs received under 50 Gy(RBE) overall.

As for the OARs areas, when one of the areas to be calculated dose distribution is close to the oriented field side on it, we find there is a near match with a slight difference in the dose calculation for both methods and a notable difference in the dose calculation for both FLUKA(RBE1.1) and Eclipse (TPS(RBE1.1)) technique in the moment the target area is far from the oriented field. This applies to all tissues except for hippocampus L, we found a difference in the calculation of the dose of both Fields as Figure 40 shows.

The presence of heterogeneity in the tissues along the pathway of filed track thus induces contradiction of calculation of the dose in both FLUKA(RBE1.1) and Eclipse (TPS(RBE1.1)) used Pencil-beam scanning technique due to in the dosimetric calculation in the Pencil-beam algorithm take into account the dose kernel inside the homogeneous tissue/medium to calculate the absorbed dose with taking consideration of the correction of inhomogeneity tissue in term of longitudinal direction in the core beam axis with ignoring the lateral scatter(Balagamwala et al., 2012). It can be said that the method of recalculating the dose by FLUKA(RBE1.1) is almost identical with Eclipse (TPS(RBE1.1)) calculation for this case of head-patient treatment kind of PTV.

By looking at the LETd consequences, the small constant difference of LETd in water phantom status, converted to the random difference at PTV and OARS, the reason is due to the nature of brain inhomogeneous medium, with LETd values remaining of Eclipse higher than FLUKA with the exception of some of the OARs as mentioned in the result section. Generally, the LETd values for organs located at a proximal range of singular fields received under 6 keV/μm and for distal range exceeded 7 keV/μm and reach in some of the OARs up

to 16 keV/μm, as estimated by FLUKA. MC code are in general more precise in low-dose regions and this could be the reason for the large difference for some OARs.
Simultaneously, RBE values increase as LETd value increases along beam penetration forward, and FLUKA calculation demonstrated RBE values higher from Eclipse Micro-Calculation on each single and both fields excluding hippocampus L side where RBE-MCN through Eclipse Micro-Calculation have high RBE value than FLUKA in the case of Both fields.
Through FLUKA calculations, the maximum of RBE reached to the 2.2 in some of the organs, whereas by Eclipse Micro-Calculation attained under 1.5.

8 Conclusion

The simulation FLUKA MC and Eclipse of water phantom shows overall relatively good agreement, similarly, in terms to patient plan, the upshots of biological dose distribution through FLUKA MC and Eclipse (TPS(RBE1.1)) exhibits agreement on the outcomes where the difference between them was most pronounced at organs located at a far distance from the singular field and a good match for both fields case except hippocampus L side.
According to both methods and through color wash distribution of LETd and RBE, some areas/organs outrange of the studied organs were exposed to the high LET and RBE value as Figures 48 and 52 illustrated of both fields.
The Micro-calculation script which was utilized by Eclipse software in order to LETd and RBE-MCN calculations gave outputs closely to the FLUKA MC in some cases and far from others, the RBE value not constant at 1.1 and increased at distal range of field.
Accordingly, the trend in the RBE values are similar to previously published results. This thesis shows that both FLUKA and Eclipse can be used to obtain LETd, but one should be aware of associated uncertainties and differences in estimates from MC and analytical methods.

Bibliograph

Ainsley, C. G., & Yeager, C. M. (2014). Practical considerations in the calibration of CT scanners for proton therapy. *Journal of applied clinical medical physics, 15*(3), 202-220.

Amato, E., Lizio, D., & Baldari, S. (2013). Applications of the Monte Carlo Method in Medical Physics. *Medical Physics,(March 2013)*, 105-113.

Anferov, V., & Das, I. J. (2015). Biological dose estimation model for proton beam therapy.

Balagamwala, E., Chao, S., & Suh, J. (2012). Principles of radiobiology of stereotactic radiosurgery and clinical applications in the central nervous system. *Technology in cancer research & treatment, 11*(1), 3-13.

Baltas, D., Sakelliou, L., & Zamboglou, N. (2006). *The physics of modern brachytherapy for oncology*: CRC Press.

Barrett, A., Morris, S., Dobbs, J., & Roques, T. (2009). *Practical radiotherapy planning*: CRC Press.

Baskar, R., Dai, J., Wenlong, N., Yeo, R., & Yeoh, K. (2014). Biological response of cancer cells to radiation treatment. Front Mol Biosci. 2014; 1: 24. In: Epub 2014/01/01. doi: 10.3389/fmolb. 2014.00024. PubMed PMID: 25988165.

Battistoni, G., Broggi, F., Brugger, M., Campanella, M., Carboni, M., Empl, A., . . . Ferrari, A. (2011). Applications of FLUKA Monte Carlo code for nuclear and accelerator physics. *Nuclear Instruments and Methods in Physics Research Section B: Beam Interactions with Materials and Atoms, 269*(24), 2850-2856.

Battistoni, G., Mattei, I., & Muraro, S. (2016). Nuclear physics and particle therapy. *Advances in Physics: X, 1*(4), 661-686.

Bethe, H. (1930). Zur theorie des durchgangs schneller korpuskularstrahlen durch materie. *Annalen der Physik, 397*(3), 325-400.

Beyzadeoglu, M., Ozyigit, G., & Ebruli, C. (2010). *Basic radiation oncology*: Springer Science & Business Media.

Beyzadeoglu, M., Ozyigit, G., & Selek, U. (2012). Radiobiology. In *Radiation Oncology* (pp. 71-135): Springer.

Bloch, F. (1933). Zur bremsung rasch bewegter teilchen beim durchgang durch materie. *Annalen der Physik, 408*(3), 285-320.

Böhlen, T., Cerutti, F., Chin, M., Fassò, A., Ferrari, A., Ortega, P. G., . . . Vlachoudis, V. (2014). The FLUKA code: developments and challenges for high energy and medical applications. *Nuclear data sheets, 120*, 211-214.

Brady, L. W., Heilmann, H., & Molls, M. (2006). *New technologies in radiation oncology*: Springer.

Bragg, W. H., & Kleeman, R. (1905). XXXIX. On the α particles of radium, and their loss of range in passing through various atoms and molecules. *The London, Edinburgh, and Dublin Philosophical Magazine and Journal of Science, 10*(57), 318-340.

Breuer, H., & Smit, B. J. (2013). *Proton therapy and radiosurgery*: Springer Science & Business Media.

Charles, M. W. (2008). ICRP Publication 103: Recommendations of the ICRP. In: Oxford University Press.

Chaturvedi, A. K., Engels, E. A., Gilbert, E. S., Chen, B. E., Storm, H., Lynch, C. F., . . . Kaijser, M. (2007). Second cancers among 104760 survivors of cervical cancer: evaluation of long-term risk. *Journal of the National Cancer Institute, 99*(21), 1634-1643.

Coutrakon, G. B. (2007). Accelerators for heavy-charged-particle radiation therapy. *Technology in cancer research & treatment, 6*(4_suppl), 49-54.

Drzymala, R., Mohan, R., Brewster, L., Chu, J., Goitein, M., Harms, W., & Urie, M. (1991). Dose-volume histograms. *International Journal of Radiation Oncology* Biology* Physics, 21*(1), 71-78.

Elia, A. (2019). *Characterization of the GATE Monte Carlo platform for non-isocentric treatments and patient specific treatment plan verification at MedAustron-Vienna-Austria.*

Eric Shinohara MD, M. (2016, November 30). Module 2: The Physics of Proton Therapy. *Energy Loss of Charged Particles in Matter, the Bragg Peak, Distal Fall off and Range Uncertainties.* Retrieved from https://www.oncolink.org/healthcare-professionals/oncolink-university/proton-therapy-professional-education/oncolink-proton-education-modules/module-2-the-physics-of-proton-therapy

Ferrari, A., Sala, P., Fasso, A., & Ranft, J. (2014). FLUKA: a multi-particle transport code (Manual). In: Stanford Linear Accelerator Center (SLAC).

Fjæra, L. F. (2016). *Development of a Monte Carlo based treatment planning verification tool for particle therapy.* The University of Bergen,

FORNELL, D. (July, 2013). An Introduction to Current Radiation Therapy Treatment Planning Systems. Retrieved from https://www.itnonline.com/article/introduction-current-radiation-therapy-treatment-planning-systems

Girdhani, S., Sachs, R., & Hlatky, L. (2013). Biological effects of proton radiation: what we know and don't know. *Radiation research, 179*(3), 257-272.

Godfrey, I. (2018). *Synthesis, structure and catalytic applications of monometallic and bimetallic gold-silver nanomaterials.* UCL (University College London),

Grassberger, C., & Paganetti, H. (2011). Elevated LET components in clinical proton beams. *Physics in Medicine & Biology, 56*(20), 6677.

Group, P. T. C.-O. Patient Statistcs. Retrieved from https://www.ptcog.ch/index.php/patient-statistics

Gui, M., Feng, Y., Yi, B., Dhople, A. A., & Yu, C. (2010). Four-dimensional intensity-modulated radiation therapy planning for dynamic tracking using a direct aperture deformation (DAD) method. *Medical Physics, 37*(5), 1966-1975.

Hawkins, M., Draper, G., & Kingston, J. (1987). Incidence of second primary tumours among childhood cancer survivors. *British journal of cancer, 56*(3), 339-347.

Hoppe, R., Phillips, T. L., & Roach, M. (2010). *Leibel and Phillips Textbook of Radiation Oncology-E-Book: Expert Consult*: Elsevier Health Sciences.

ICRU, L. E. T. Report 16, International Commis-sion on Radiation Units and Measurements, Washington, DC, 1970. *IcruLinear Energy Transfer1970*.

Institute, N. C. (2019,July). How Cancer Is Diagnosed. Retrieved from https://www.cancer.gov/about-cancer/diagnosis-staging/diagnosis

Jaffray, D. A. (2012). Image-guided radiotherapy: from current concept to future perspectives. *Nature Reviews Clinical Oncology, 9*(12), 688.

Jones, B. (2015). Towards achieving the full clinical potential of proton therapy by inclusion of LET and RBE models. *Cancers, 7*(1), 460-480.

Jones, D. (1994). ICRU report 50—prescribing, recording and reporting photon beam therapy. *Medical physics, 21*(6), 833-834.

Khan, F. M., & Gibbons, J. P. (2014). *Khan's the physics of radiation therapy*: Lippincott Williams & Wilkins.

Lawrence, J. H. (1957). Proton irradiation of the pituitary. *Cancer, 10*(4), 795-798.

Lomax, A. J. (2009). Charged particle therapy: the physics of interaction. *The Cancer Journal, 15*(4), 285-291.

Mayles, P., Nahum, A., & Rosenwald, J.-C. (2007). *Handbook of radiotherapy physics: theory and practice*: CRC Press.

McMahon, S. J. (2018). The linear quadratic model: usage, interpretation and challenges. *Physics in Medicine & Biology, 64*(1), 01TR01.
Mohan, R., Mahajan, A., & Minsky, B. D. (2013). New strategies in radiation therapy: Exploiting the full potential of protons. *Clinical Cancer Research, 19*(23), 6338-6343.
Mori, Y., Sakae, T., Takada, K., & Takei, H. (2020). Treatment Planning System for Proton Radiotherapy. In *Proton Beam Radiotherapy* (pp. 113-125): Springer.
National Cancer Institute. (2015). What Is Cancer. Retrieved from https://www.cancer.gov/about-cancer/understanding/what-is-cancer
Newhauser, W. D., & Zhang, R. (2015). The physics of proton therapy. *Physics in Medicine & Biology, 60*(8), R155.
Paganetti, H. (2002). Nuclear interactions in proton therapy: dose and relative biological effect distributions originating from primary and secondary particles. *Physics in Medicine & Biology, 47*(5), 747.
Paganetti, H. (2003). Significance and implementation of RBE variations in proton beam therapy. *Technology in Cancer Research & Treatment, 2*(5), 413-426.
Paganetti, H. (2009). Dose to water versus dose to medium in proton beam therapy. *Physics in Medicine & Biology, 54*(14), 4399.
Paganetti, H. (2018). *Proton therapy physics*: CRC press.
Paganetti, H., Niemierko, A., Ancukiewicz, M., Gerweck, L. E., Goitein, M., Loeffler, J. S., & Suit, H. D. (2002). Relative biological effectiveness (RBE) values for proton beam therapy. *International Journal of Radiation Oncology* Biology* Physics, 53*(2), 407-421.
Park, S. H., & Kang, J. O. (2011). Basics of particle therapy I: physics. *Radiation oncology journal, 29*(3), 135.
Pinter, C., Lasso, A., Wang, A., Jaffray, D., & Fichtinger, G. (2012). SlicerRT: radiation therapy research toolkit for 3D Slicer. *Medical physics, 39*(10), 6332-6338.
Report 16. (2016). *Journal of the International Commission on Radiation Units and Measurements, os9*(1), NP-NP. doi:10.1093/jicru/os9.1.Report16
Report 90. (2016). *Journal of the International Commission on Radiation Units and Measurements, 14*(1), NP-NP. doi:10.1093/jicru/ndw043
Rydberg, B. (1996). Clusters of DNA damage induced by ionizing radiation: formation of short DNA fragments. II. Experimental detection. *Radiation research, 145*(2), 200-209.
Seco, J., & Verhaegen, F. (2013). *Monte Carlo techniques in radiation therapy*: CRC press.
Smith, N. B., & Webb, A. (2010). *Introduction to medical imaging: physics, engineering and clinical applications*: Cambridge university press.
Song, C. W., Park, H., Griffin, R. J., & Levitt, S. H. (2011). Radiobiology of stereotactic radiosurgery and stereotactic body radiation therapy. In *Technical basis of radiation therapy* (pp. 51-61): Springer.
Takei, H. (2020). Physical Characteristics of Proton Beams. In *Proton Beam Radiotherapy* (pp. 37-50): Springer.
Tayama, R., Handa, H., Hayashi, K., Nakano, H., Sasamoto, N., Nakashma, H., & Masukawa, F. (2002). Benchmark calculations of neutron yields and dose equivalent from thick iron target for 52–256 MeV protons. *Nuclear engineering and design, 213*(2-3), 119-131.
Teoh, M., Clark, C., Wood, K., Whitaker, S., & Nisbet, A. (2011). Volumetric modulated arc therapy: a review of current literature and clinical use in practice. *The British journal of radiology, 84*(1007), 967-996.
Thomas, D. J. (2012). ICRU report 85: fundamental quantities and units for ionizing radiation. In: Oxford University Press.

Tsuboi, K. (2020). Early History of Biology and Clinical Application of Proton Beam Therapy. In *Proton Beam Radiotherapy* (pp. 9-21): Springer.
Tsuboi, K., Sakae, T., & Gerelchuluun, A. (2020). *Proton Beam Radiotherapy: Physics and Biology*: Springer.
Units, I. C. o. R. (1998). *Fundamental quantities and units for ionizing radiation* (Vol. 60): International Commission on Radiation.
Use, R. S. (2008). Replacement: Abbreviated Version. *Nuclear and Radiation Studies Board. Division on Earth*.
Varian. (2015). Eclipse Proton Algorithms Reference Guide.
Verburg, J. M., Grassberger, C., Dowdell, S., Schuemann, J., Seco, J., & Paganetti, H. (2016). Automated Monte Carlo simulation of proton therapy treatment plans. *Technology in cancer research & treatment, 15*(6), NP35-NP46.
Wambersie, A., Hendry, J., Andreo, P., DeLuca, P., Gahbauer, R., Menzel, H., & Whitmore, G. (2006). The RBE issues in ion-beam therapy: conclusions of a joint IAEA/ICRU working group regarding quantities and units. *Radiation protection dosimetry, 122*(1-4), 463-470.
Wambersie, A., Menzel, H., Andreo, P., DeLuca Jr, P., Gahbauer, R., Hendry, J., & Jones, D. (2011). Isoeffective dose: a concept for biological weighting of absorbed dose in proton and heavier-ion therapies. *Radiation protection dosimetry, 143*(2-4), 481-486.
Webb, S. (1997). *The physics of conformal radiotherapy: advances in technology (PBK)*: CRC Press.
Wilkens, J. J., & Oelfke, U. (2003). Analytical linear energy transfer calculations for proton therapy. *Medical physics, 30*(5), 806-815.
Willers, H., Allen, A., Grosshans, D., McMahon, S. J., von Neubeck, C., Wiese, C., & Vikram, B. (2018). Toward A variable RBE for proton beam therapy. *Radiotherapy and Oncology, 128*(1), 68-75.
Wilson, R. R. (1946). Radiological use of fast protons. *Radiology, 47*(5), 487-491.
World Health Organization. (2018,September). Cancer. Retrieved from https://www.who.int/news-room/fact-sheets/detail/cancer
Yamoah, K., & Johnstone, P. A. (2016). Proton beam therapy: clinical utility and current status in prostate cancer. *OncoTargets and therapy, 9*, 5721.
Zirkle, R. E., Marchbank, D. F., & Kuck, K. D. (1951). *Exponential and sigmoid survival curves resulting from alpha and x irradiation of Aspergillus spores*. Retrieved from